JOURNAL OF GEOPHYSICAL RESEARCH, VOL. 93, NO. A3, PAGES 1871–1895, MARCH 1, 1988

Electron Density Depletions in the Nightside Auroral Zone

A. M. PERSOON,[1] D. A. GURNETT,[1] W. K. PETERSON,[2] J. H. WAITE, JR.,[3] J. L. BURCH,[4] AND J. L. GREEN[5]

Measurements from instruments on board Dynamics Explorer 1 are used to study regions of diminished electron density in the nightside auroral zone. Local electron densities are obtained from the electron plasma frequency cutoff of the whistler mode auroral hiss. Electron density profiles are highly variable through the nightside auroral zone. Sharply defined regions of low electron densities are a common feature of auroral zone crossings from the predusk hours until the early morning hours at all radial distances up to at least 4.6 R_E. Electron densities in these regions are strongly depleted in relation to the adjacent polar cap and plasmaspheric densities, forming a low-density cavity at 70° ± 5° invariant latitude. Minimum densities in the auroral cavity frequently fall to values below 0.3 cm^{-3} and rarely exceed 3 cm^{-3} at radial distances of 2–4.6 R_E. Within the cavity the electron density profile exhibits extreme variability, with variations of a factor of 2 or more on spatial scales of tens of kilometers. Electron plasma frequency to electron cyclotron frequency ratios of 0.02–0.4 are found inside the auroral cavity, consistent with the values required by theory for the generation of auroral kilometric radiation and Z mode radiation. A comparison of the electron density depletions with simultaneously measured low- and high-energy particle measurements indicates a correspondence between low auroral plasma densities and upward directed ion beams and conics. Low-energy (<1 keV) upflowing H^+ ions are strongly correlated with the poleward edge of the auroral cavity. Although the energetic (>1 keV) precipitating auroral electrons do not correlate with the poleward edge of the auroral cavity, the peak energies of the precipitating electron population do occur inside the cavity interval. These correlations show that density depletions in the nightside auroral zone are directly associated with auroral acceleration processes.

1. INTRODUCTION

The purposes of this study are to examine electron density depletions which occur on nightside auroral field lines at geocentric radial distances of 2–4.7 R_E, to determine whether the minimum densities found inside these depletions are consistent with those required by theory for the generation of auroral kilometric radiation (AKR) and Z mode radiation, and to correlate these depletions with the observed auroral particle distributions.

The occurrence of electron density enhancements and depletions at polar and middle latitudes was the subject of thorough investigation in the 1960s and early 1970s. The focus of much of the early, low-altitude studies was a mid-latitude minimum in the electron density, first detected in ground-based ionosonde data at the peak of the F layer [*Reber and Ellis*, 1956]. This density minimum was found to occur during the nighttime hours between 50° and 60° geomagnetic latitude. Early measurements from the topside sounder Alouette 1 confirmed the existence of a consistent electron density trough along a circular arc at 60° geomagnetic latitude centered on the geomagnetic pole [*Muldrew*, 1965]. Ground-based ionosonde data and ion trap data were used to verify the existence of the trough just below and just above the peak of the F layer, hinting at the field-aligned nature of this phenomenon over a large altitude range [*Sharp*, 1966; *Stanley*, 1966; *Bowman*, 1969].

To extend the study of electron density depletions to higher altitudes, topside sounder data from the Alouette 1 satellite and in situ probe measurements from the Ariel and Explorer satellites were used to determine the geomagnetic influence on the trough position and its seasonal and diurnal variations up to 1000 km [*Muldrew*, 1965; *Thomas et al.*, 1966; *Nelms*, 1966; *Nishida*, 1967; *Rycroft and Thomas*, 1970; *Tulunay and Sayers*, 1971; *Tulunay*, 1972; *Brace and Reddy*, 1965; *Calvert*, 1966; *Brace et al.*, 1968; *Miller and Brace*, 1969; *Miller*, 1970]. The trough was also observed in total electron content data [*Liszka*, 1967], indicating that the trough existed along geomagnetic field lines up to 1000 km and was not a local phenomenon due to a transient redistribution of ionization. Above 1000 km, topside sounder data from the Alouette 2 and ISIS 1 satellites were used to confirm the location and variations in the mid-latitude trough up to 3600 km [*Hagg*, 1967; *Nelms and Lockwood*, 1967; *Timleck and Nelms*, 1969; *Brace and Theis*, 1974].

Although the low-latitude boundary of the main electron trough was easily confirmed by direct and indirect measurements at all altitudes up to 3600 km, density features poleward of the trough were found to be transient and very irregular [*Brace and Reddy*, 1965; *Muldrew*, 1965]. Very low electron densities were detected at all latitudes and local times above the main trough in the Alouette and Explorer data [*Thomas et al.*, 1966; *Hagg*, 1967; *Nelms and Lockwood*, 1967; *Miller and Brace*, 1969; *Timleck and Nelms*, 1969]. Although some studies indicated that a region of enhanced densities with steep density gradients formed a poleward edge of the main trough [*Sharp*, 1966; *Calvert*, 1966; *Nishida*, 1967; *Miller and Brace*, 1969; *Bates et al.*, 1973], these auroral enhancements were often found to be highly irregular in shape and variable in location, leading some to conclude that the auroral enhancements were merely transient density structures superimposed on a stable

[1]Department of Physics and Astronomy, University of Iowa, Iowa City.
[2]Lockheed Missiles and Space Company, Inc., Palo Alto, California.
[3]Space Science Laboratory, NASA Marshall Space Flight Center, Huntsville, Alabama.
[4]Department of Space Sciences, Southwest Research Institute, San Antonio, Texas.
[5]National Space Science Data Center, NASA Goddard Space Flight Center, Greenbelt, Maryland.

Paper number 6A8885.
0148-0227/88/006A-8885$05.00

region of depressed polar densities [*Nishida*, 1967; *Miller and Brace*, 1969].

In an effort to determine a pattern in the highly variable and complex high-latitude density profile at 1000 km, *Thomas and Andrews* [1968] sampled the electron densities along a line at a fixed angle to the Earth-Sun line. Characteristic patterns in the electron maxima and minima in invariant latitude and local time suggested a division of the high-latitude magnetosphere into two density zones [*Thomas and Andrews*, 1968; *Andrews and Thomas*, 1969; *Miller and Brace*, 1969]. The crescent-shaped mid-latitude zone containing the main trough had a well-defined low-latitude boundary at the plasmapause [*Andrews and Thomas*, 1969] and a high-latitude boundary several degrees equatorward of the auroral oval [*Bates et al.*, 1973]. The polar zone, a region of open field lines and depressed electron densities spreading over the entire polar cap, was elliptical and slightly skewed toward local midnight [*Andrews and Thomas*, 1969]. The auroral oval, the transition region between the two zones, was found to be enclosed in the enhanced density region, bounded at low latitudes by the poleward edge of the main trough and at high latitudes by the highly variable boundary separating the enhanced auroral densities and the depressed polar densities [see *Andrews and Thomas*, 1969, Figure 4].

In the low-altitude auroral region of enhanced electron densities, recent studies have found evidence of high-latitude ion troughs (HLTs) at altitudes below 1000 km. These troughs were identified as depletions of atomic ions, accompanied by abrupt enhancements in the molecular ions, near 70° magnetic latitude in the auroral zone [*Taylor et al.*, 1975; *Grebowsky et al.*, 1976, 1983]. The HLTs were distinguished from the light ion troughs associated with Muldrew's electron density trough, although the two types of ion depletions would tend to merge under certain diurnal and seasonal conditions [*Taylor et al.*, 1975]. No similar, persistent pattern of electron density depletions was found inside the auroral zone below 2000 km.

Above 2000 km a different picture of auroral electron densities emerged. In the last decade, one focus of studies involving auroral plasma densities has been the generation of auroral kilometric radiation. The generation of AKR requires low plasma densities in the auroral source region [*Melrose*, 1976; *Wu and Lee*, 1979; *Grabbe et al.*, 1980; *James*, 1980]. Using ISIS 1 topside sounder data, *Benson and Calvert* [1979] investigated the low-altitude portion of the AKR source region from 2400 km to 3500 km and found that the source region was embedded within local electron density depletions in the nightside auroral zone. Electron densities in the source region fell below 100 cm^{-3}, orders of magnitude below the ambient plasma densities poleward and equatorward of the depletion. Occasionally sharp electron density enhancements were found within the source region depletions. The density-height profiles indicated that the enhancements extended far down into the ionosphere [*Benson and Calvert*, 1979]. However, the broader density depletions were limited to altitudes above 2000 km [*Benson and Calvert*, 1979; *Benson and Akasofu*, 1984]. Using complete electron density contours from the height of ISIS 1 near apogee down to the F region ionization peak, *Benson and Akasofu* [1984] found that the AKR source region density depletions varied in latitudinal extent from a few degrees to tens of degrees.

The auroral zone above 2 R_E is an important region in the study of auroral physics and particle acceleration. It is a region of parallel electric fields and field-aligned currents, of inverted-V electron precipitation, ion conic distributions, and field-aligned ion beams, of intense AKR, Z mode radiation, and auroral hiss emissions. The interrelationships of these auroral phenomena have been extensively studied for decades, and some, such as AKR generation, have been correlated with low auroral plasma densities below 2 R_E. Studies of density structures in the auroral zone at higher altitudes became possible with the launch of two polar-orbiting spacecraft in the late 1970s. *Calvert* [1981] used electron densities obtained from the electric field measurements of the Hawkeye 1 spacecraft to verify the existence of an auroral plasma cavity at an invariant latitude of 70° ± 3° inside the AKR source region up to 3 R_E geocentric. In situ density measurements from the S3-3 satellite confirmed the existence of this density cavity at 2.1 R_E geocentric [*Temerin*, 1984]. Further examples of low electron densities were found in the S3-3 data in association with electrostatic shocks and parallel electric fields [*Mozer et al.*, 1977; *Mozer and Temerin*, 1983] and in association with field-aligned ion beams [*Temerin et al.*, 1981].

The Dynamics Explorer 1 spacecraft, with its high-frequency resolution and spatial coverage in the auroral zone, is in an excellent position to extend the study of auroral plasma densities in this very important region of the magnetosphere. DE 1, launched on August 3, 1981, is in an eccentric polar orbit with perigee and apogee geocentric radial distances of 1.09 R_E and 4.66 R_E, respectively. This study uses data from the plasma wave instrument (PWI) acquired during the first 8 months of the DE 1 mission, from September 1981 to April 1982. During this period the latitudinal precession of the DE orbit enabled the spacecraft to accumulate data in the nightside auroral zone over geocentric radial distances of 2 R_E to 4.7 R_E in the northern hemisphere and 1.1 R_E to approximately 3 R_E in the southern hemisphere.

Electric field spectrum measurements from the PWI have been used to derive electron densities in the auroral zone. The plasma wave instrument on DE 1 has been described in detail in a previous report [see *Shawhan et al.*, 1981]. Signals from the 200-m (tip-to-tip) electric antenna, oriented perpendicular to the spacecraft spin axis, are processed by two frequency correlators which scan a frequency range of 1.78 Hz to 400 kHz once every 32 s. The resulting electric field amplitude measurements are displayed in frequency-time spectrogram form (see Figures 1, 3, 4, and 11) and used in the determination of auroral electron densities.

Analog data from the PWI wideband instrument are used in this study to acquire high time and frequency resolution for the analysis of auroral electron densities and the identification of fine structure in the auroral density profile. Since the density analysis technique used in this study requires precise measurements of the auroral hiss cutoff (usually below 40 kHz), wideband analog data were used with either a 10-kHz or a 40-kHz bandwidth. The wideband signals are processed through a spectrum analyzer with 512 frequency channels and 40-ms time resolution and displayed on film.

Observations from the energetic ion composition spectrometer, the retarding ion mass spectrometer, and the high-altitude plasma instrument are brought together with the plasma wave measurements to determine the composition and behavior of the auroral ions and electrons inside the

auroral cavity. The energetic ion composition spectrometer (EICS) is a high-resolution ion mass spectrometer, designed to measure the energy and pitch angle distributions of ions in a mass range of <1 amu/e to 150 amu/e in 64 mass channels. The energy range of the ions spans 0 eV (spacecraft potential) to 17 keV/e in 32 energy steps. The field of view of the instrument is perpendicular to the spacecraft spin axis and provides complete pitch angle coverage every spacecraft rotation. The instrument is described in detail by *Shelley et al.* [1981].

The retarding ion mass spectrometer (RIMS), consisting of three sensor heads, three retarding potential analyzers, and a magnetic ion mass spectrometer, is designed to measure low-energy ions with energies from 0 eV (spacecraft potential) to 50 eV in a mass range of 1 to 32 amu. In this study, data from the radial sensor head, perpendicular to the spacecraft spin axis, are used to determine the angular distributions of the low-energy ions with respect to the ambient magnetic field. A complete description of the instrument is given by *Chappell et al.* [1981].

The high-altitude plasma instrument (HAPI) consists of five electrostatic analyzers with five viewing angles distributed from 45° to 135° relative to the spacecraft spin axis. HAPI provides simultaneous measurements of electrons and ions in the energy per charge range of 5 eV to 32 keV. The instrument is described in detail by *Burch et al.* [1981].

2. Density Analysis Technique

2.1. *The Determination of the Electron Density*

DE 1 electron density measurements have been determined from an analysis of whistler mode wave propagation using electric field spectrum measurements from the plasma wave instrument. The PWI electric field amplitude measurements are displayed in frequency-time spectrogram form. Each spectrogram covers a 2-hour time interval and spans a frequency range of 1.78 Hz to 400 kHz. A typical example of an electric field spectrogram illustrating a pass through the nightside polar cap and auroral zone is shown in Figure 1. The intense emissions below 30 kHz which spread out from the auroral zone toward the pole are auroral hiss emissions. On the spectrogram these hiss emissions appear to have a sharp upper frequency cutoff between 20 kHz and 30 kHz. According to cold plasma theory, a whistler mode wave, propagating parallel to the magnetic field, will resonate at either the electron cyclotron frequency (f_{ce}) or the electron plasma frequency (f_{pe}) [see *Helliwell*, 1965, Figure 3-2]. In the low-density polar cap and auroral regions where $f_{pe} \ll f_{ce}$, parallel-propagating whistler mode auroral hiss emissions will resonate at the electron plasma frequency.

In Figure 1 the electron plasma frequency varies from 20 to 30 kHz in the polar cap and drops to 7 kHz in the auroral zone. The electron plasma frequency is determined by tracing the upper frequency cutoff of the auroral hiss emissions with a manually controlled cursor against a spectrogram displayed on a video monitor. A frequency value is recorded for each 32-s sweep of the step frequency correlator. In addition, orbit parameters of the spacecraft, such as L shell and magnetic latitude, are recorded for each frequency value and are used to construct the latitudinal density profiles. The electron density is calculated from the electron plasma frequency by using the relation $n_e = (f_{pe}/9)^2$, where n_e is in cm^{-3} and f_{pe} is in kilohertz. This density analysis technique and its limitations have been fully described by *Persoon et al.* [1983]. The determination of the electron density from the electron plasma frequency is a valuable method of determining the total plasma density and is independent of the energies of the auroral plasma population.

2.2. *Factors Limiting the Technique*

This technique permits the determination of the electron density to a high degree of accuracy. When the auroral hiss propagates parallel to the magnetic field, the hiss amplitude will exhibit a steep amplitude gradient at the local electron plasma frequency. Under these conditions the accuracy in determining the electron density is limited primarily by the size of the discrete frequency steps sampled by the step frequency correlator. At 20 kHz, a typical frequency cutoff value in the polar cap, the electron plasma frequency can be determined within ±1.3 kHz, corresponding to an uncertainty in the density determination of ±13%. However, this error is not sufficient to account for the typical difficulties involved in digitizing the upper frequency cutoff of the hiss emissions in the auroral zone. The most troublesome difficulty is the presence of other intense emissions propagating in the 1- to 100-kHz frequency range at auroral latitudes. These include broadband electrostatic emissions, Z mode radiation, and AKR, all of which propagate in overlapping frequency ranges in the auroral zone [*Gurnett et al.*, 1983]. Frequently, these emissions are intense enough to obscure the cutoff of the auroral hiss emissions. Since incorrect wave mode identification can result in significant density errors, no density data were recorded for those intervals in which the whistler mode amplitude was not continuous and sufficiently enhanced above the amplitudes of competing wave modes near the resonance frequency.

Another significant source of error in the auroral density determination is the identification of the upper frequency cutoff of the auroral hiss emissions with the local electron plasma frequency. The resonance frequency of a whistler mode wave is at the electron plasma frequency only when the wave is propagating parallel to the magnetic field at resonance [*Helliwell*, 1965]. The technique of using the upper cutoff frequency of auroral hiss emissions to derive electron densities is based on the assumption that the whistler mode wave is propagating at very small angles to the magnetic field near resonance. These upgoing hiss emissions are believed to be propagating at wave normal angles very close to the resonance cone [*Mosier and Gurnett*, 1969; *Smith*, 1969; *Gurnett and Frank*, 1972; *James*, 1976]. Using geometric constructions to analyze the ray path of upward propagating auroral hiss emissions, *Gurnett et al.* [1983] have shown that the wave angle tends to approach zero as the wave frequency approaches the electron plasma frequency [see *Gurnett et al.*, 1983, Figure 10]. The details of the whistler mode ray path will actually determine whether the wave will reach resonance at the electron plasma frequency or at a lower resonance frequency. The whistler mode ray path in the auroral zone is discussed in detail below (see Figure 2).

A further problem in identifying the upper frequency cutoff with the electron plasma frequency exists because hot plasma effects such as cyclotron damping and Landau damping can cause the whistler mode to be strongly attenuated at

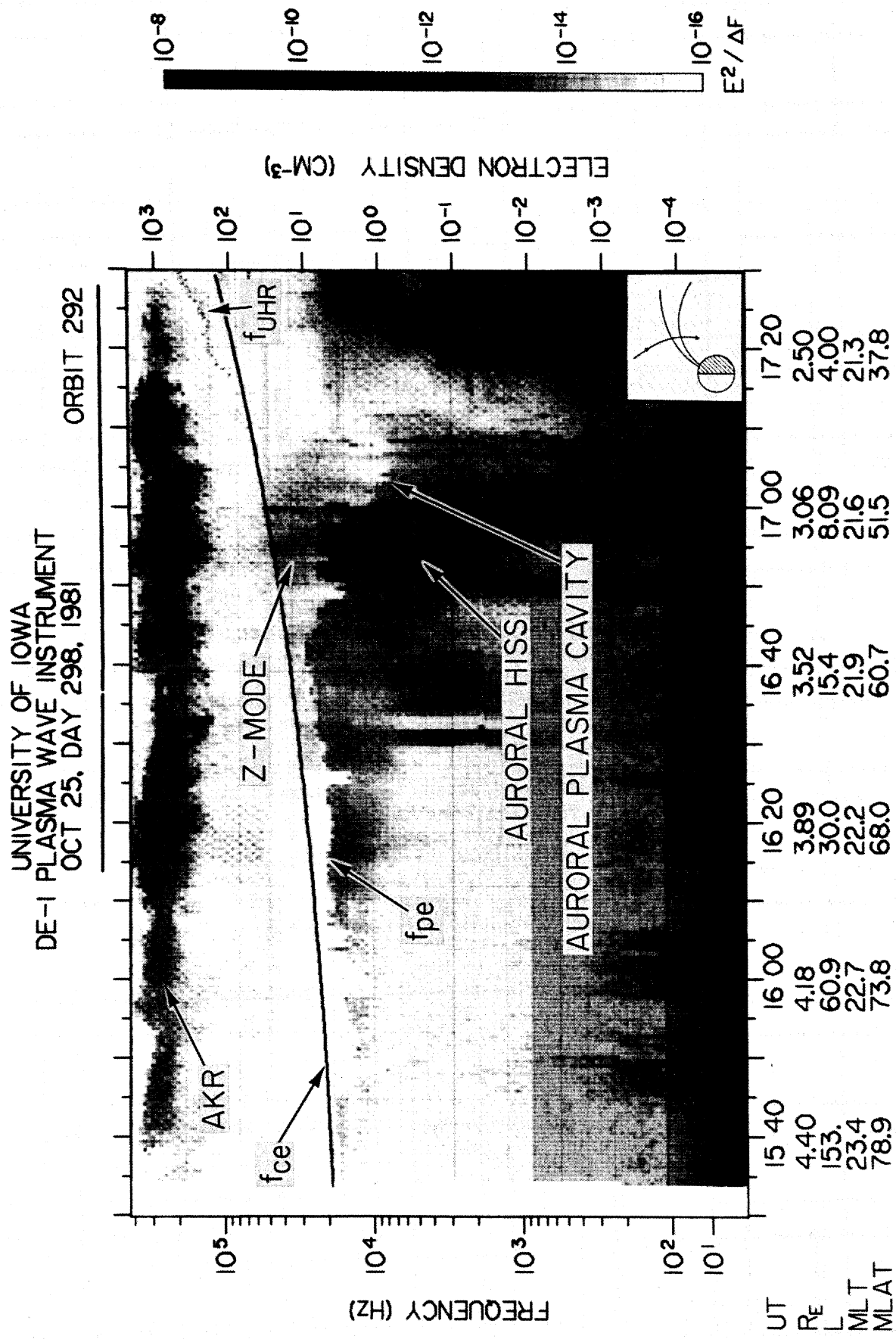

Fig. 1. A representative spectrogram of electric field amplitude measurements illustrating a pass through the nightside polar cap and auroral zone on October 25, 1981. The trajectory of the spacecraft in a magnetic meridian plane is shown in the lower right-hand corner. The density scale is along the right vertical axis. The auroral cavity is encountered at 1700 UT. The f_{UHR} emissions, which are commonly faint features in the high-frequency data, have been selectively enhanced to preserve the wave features through the photographic reproduction process.

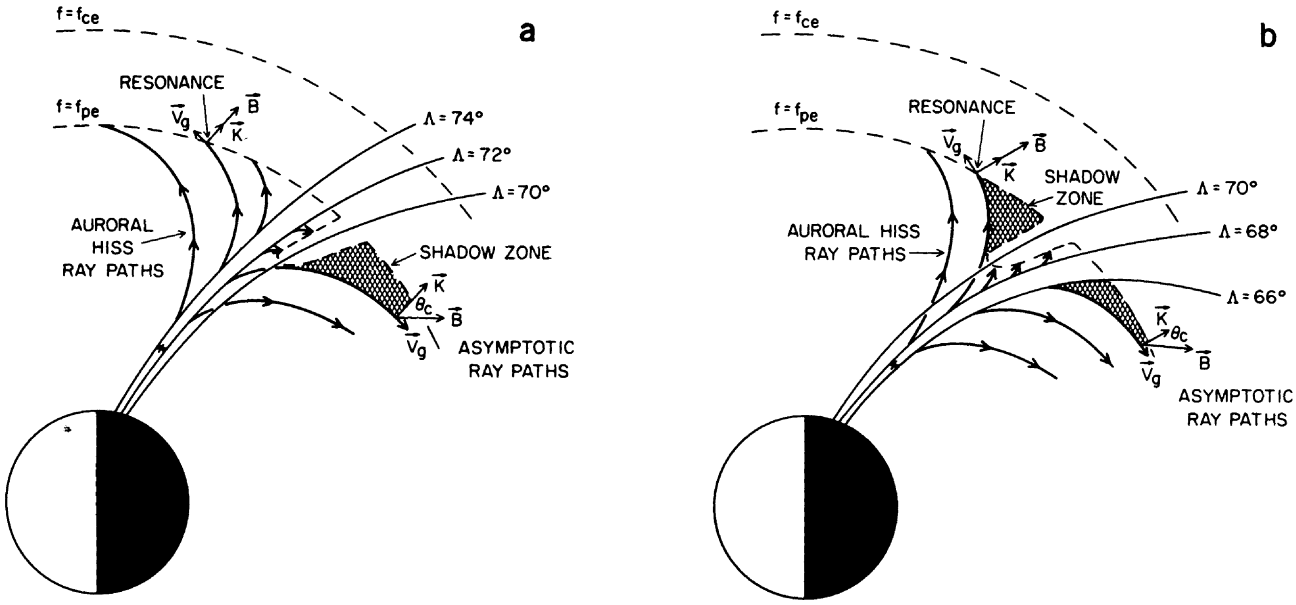

Fig. 2. A qualtitative representation of the upward propagating auroral hiss emissions from a source region below and poleward of the low-density field lines (Figure 2*a*) and from a source region equatorward of the low-density field lines (Figure 2*b*). No resonance occurs in the region where the ray paths are oblique with respect to the contours of constant electron plasma frequency.

frequencies below the electron plasma frequency. Because of the typically low auroral densities presented in this study, the electron plasma frequency is always well below the electron cyclotron frequency, except occasionally at the cavity edges. Therefore cyclotron damping is expected to be an insignificant factor in the analysis of auroral density troughs. However, Landau resonance is a significant factor whenever a hot energetic component is present in the plasma. Energetic particles with velocities approaching the wave phase velocity can absorb energy from the wave and cause a gradual decline in the amplitude of the hiss emissions below the electron plasma frequency. Under these conditions, density values derived from the poorly defined upper frequency cutoff will be too low.

The appearance of the auroral cavity on the PWI spectrograms presents a further difficulty in locating the upper frequency cutoff. The amplitude gradient of the hiss emissions at the upper frequency cutoff varies as the whistler mode wave propagates to higher and lower latitudes away from the source region. In an earlier study, it has been shown that the characteristic funnel shape of the hiss emissions is the result of the upward propagation of whistler mode waves above the source region [see *Gurnett et al.*, 1983, Figures 10 and 11]. Poleward of the source region the whistler mode waves are driven into resonance at a sharp upper frequency cutoff, identified as the electron plasma frequency [*Persoon et al.*, 1983]. The amplitude gradient of the hiss emissions defines the upper frequency cutoff. Equatorward of the source field lines the whistler mode wave propagates at large angles to the magnetic field lines, resulting in a poorly defined upper frequency cutoff and a fuzzy appearance on the spectrogram. In this region the hiss emissions will not resonate at the local electron plasma frequency. The upper frequency limit for the propagation of the hiss emissions in this region may be caused by electron density variations along the ray path and not by local electron density conditions. Directly above the source region the propagation of the whistler mode emissions into a region of field-aligned diminished plasma densities produces the characteristic appearance of the auroral cavity in the PWI data.

Figure 2*a* is a qualitative representation of the upward propagating auroral hiss emissions from a source region below and poleward of the low-density field lines. The poleward propagating whistler mode waves will be driven into resonance at the local electron plasma frequency poleward of the density cavity. The latitudinal density profile, which is derived from the digitized resonance frequency, will exhibit a steep gradient at the poleward boundary of the low-density region. However, a shadow zone, where the equatorward propagating whistler mode waves are not driven into resonance at the local electron plasma frequency, will occur equatorward of the density structure. The electron density cannot be determined in this shadow zone because the cutoff is not representative of the local density conditions. In Figure 1 the shadow zone is responsible for the termination of the auroral density profile at 1707 UT.

Figure 2*b* illustrates the opposite effect, when the auroral hiss source region is located on field lines below and equatorward of the low-density field lines. In this case, the shadow zone will occur poleward of the cavity, obscuring the poleward edge of the plasma cavity. A sudden increase in the resonance frequency will result in a sharp density gradient at the equatorward edge of the cavity. However, the propagation of the hiss emissions at increasingly larger angles to the magnetic field equatorward of the source field lines will produce a second shadow zone in this region. Figure 2*b* represents the expected whistler mode propagation for a source located near the equatorward edge of the auroral zone. In Figure 4*b* a sharp increase in the upper frequency cutoff of the hiss emissions at 0637 UT and 0813 UT defines the equatorward edge of the main auroral cavity in both hemispheres. This is not typical, however. A sharp,

well-defined equatorward edge is not usually observed in most of the auroral cavity events.

The finite latitudinal width of the auroral hiss source region will control the size of the shadow zone resonance effect at the walls of the cavity. Since the location of the auroral hiss source region varies with changing magnetospheric conditions, the appearance of the auroral cavity in the PWI data will vary between the two extremes presented in Figure 2. An inspection of the 74 auroral cavities assembled for this study indicates that a well-defined upper frequency cutoff at the poleward edge of the cavity is nearly always observed in the PWI data. However, a well-defined and increasing upper frequency cutoff near the equatorward edge of the cavity is only observable on approximately 44% of the DE auroral cavity examples. The lack of evidence for a well-defined equatorward edge of the auroral cavity is probably due to the effects of the propagation of auroral hiss emissions across the low-density field lines and does not indicate the absence of an equatorward edge. In at least 39% of the examples with no well-defined equatorward edge, there is evidence of a rapidly increasing upper hybrid resonance frequency at lower invariant latitudes, indicating that the auroral cavity is a U-shaped density structure with density gradients at both walls of the cavity.

2.3. *Estimation of Error*

Typically, it is more difficult to determine the auroral hiss cutoff frequency at auroral latitudes than at polar latitudes. The minimum error in locating the frequency cutoff in the PWI auroral zone data is estimated to be ±2 frequency steps of the step frequency correlator. At 8 kHz, a typical electron plasma frequency in the auroral zone, the upper frequency cutoff can be determined within ±1.1 kHz, corresponding to an uncertainty in the density determination of ±27%. The upper frequency cutoff was not digitized if the uncertainty exceeded ±3 frequency steps, corresponding to a maximum uncertainty in the density determination of ±40%.

3. OBSERVATIONS

To study the electron density depletions located on nightside auroral field lines, PWI spectrograms from the first 8 months of the DE mission were assembled for which continuous data coverage was available from the polar cap to the plasmasphere. The various regions of the magnetosphere were identified from a combination of the spacecraft's orbit parameters and the characteristic wave signatures in each region. The polar cap was identified by the wave signature of the poleward propagating auroral hiss [*Persoon et al.*, 1983]. The plasmasphere was identified on the PWI spectrograms by the wave signatures of the plasmaspheric hiss and chorus emissions and, whenever possible, by the simultaneous observation of the upper hybrid resonance, indicating elevated plasma densities on closed field lines.

The characteristic funnel shape of the auroral hiss emissions observed on the PWI spectrograms for many nightside auroral zone crossings [*Gurnett et al.*, 1983] was not used as the sole determining factor in assembling auroral zone data. This decision was made for two reasons. Recently, it has been found that funnel-shaped auroral hiss emissions can occur at high polar latitudes in connection with theta aurorae [*Frank et al.*, 1986]. Even at auroral latitudes the funnel shape of the hiss emissions is not evident on all nightside auroral zone crossings. At lower altitudes just above the auroral hiss source region, the poleward and equatorward expansions of the auroral hiss emissions are not observed on the spectrograms owing to the 400-kHz cutoff of the step frequency receiver and to the convergence of the L shells at low altitudes. However, even on these low-altitude passes there is an identifiable auroral hiss signature in the form of intense broadband electromagnetic emissions spatially confined to the auroral field lines.

3.1. *Representative Auroral Cavities*

Characteristic plasma wave signatures for all three regions of the magnetosphere were used in combination with the spacecraft orbit parameters to collect spectrograms of auroral zone crossings for which continuous data coverage through the auroral zone was available. Typical spectrograms from this data base are presented to illustrate the appearance of the auroral cavity in the PWI data. The density scale is located along the right vertical axis, and the trajectory of the spacecraft in a magnetic meridian plane is shown in the lower corner.

Day 298, 1981. A typical example of a nightside auroral cavity in the northern hemisphere is illustrated in Figure 1 for October 25, 1981. The characteristic funnel-shaped auroral hiss emissions can be seen propagating poleward from the nightside auroral region below 26 kHz. The main auroral cavity begins at 1700 UT. Z mode radiation, found both inside and poleward of the cavity, can be seen up to the electron cyclotron frequency, and intense AKR is found over much of this interval above 120 kHz. The electron density profile, derived from the electron plasma frequency cutoff, is smoothly varying over most of this interval. The Kp index for this pass is 2+.

As the spacecraft approaches the auroral region, several small density depressions can be seen at 1625 UT and 1648 UT. These small depletions have sharply defined poleward and equatorward edges and minimum densities that are a half order of magnitude higher than the minimum densities found inside the main cavity. High-latitude density depletions just poleward of the main auroral cavity are common features in the PWI spectrograms. A modest 39% drop in the electron density at 1658 UT precedes the main cavity. When the spacecraft encounters the main cavity at 1700 UT, there is a substantial 87% drop in the density profile below the average polar cap density values. Typically, the minimum density values found inside the auroral cavity are nearly an order of magnitude lower than the density values just poleward of the cavity. In this example, the average electron density just poleward of the cavity (1656–1657 UT) is 5.1 cm^{-3}. The minimum cavity density of 0.65 cm^{-3} occurs at 1704 UT and is nearly an order of magnitude below the polar cap values. The amplitude of the whistler mode wave falls off with decreasing latitude and increasing frequency after 1707 UT. In this region equatorward of the hiss source field lines, the auroral hiss emissions do not resonate at the local electron plasma frequency (see section 2.2). However, the faint f_{UHR} emissions equatorward of the cavity make it possible to construct the electron density profile after 1718 UT. At 1718 UT the measured electron density is 72 cm^{-3}, nearly 2 orders of magnitude above the last measured cavity value of 0.87 cm^{-3} at 1707 UT. This sharp increase would indicate that the auroral cavity is a U-shaped density structure, even though the equatorward edge of the density cavity cannot be accurately determined.

Day 303, 1981. The spectrogram for October 30, 1981, in Figure 3*a* has been chosen to illustrate the variability in the electron density profile inside the cavity. This pass is significant for the enhanced wave activity at all frequencies and for the highly variable density profile both inside and outside the cavity. The *Kp* index for this pass is 4−. The spacecraft is approaching the auroral zone from the nightside polar cap. Again the characteristic funnel-shaped auroral hiss emissions can be seen propagating poleward from the auroral zone below 20 kHz. Unlike the pass illustrated in Figure 1, the electron plasma frequency cutoff of the hiss emissions, even deep inside the polar cap, is highly variable. The spacecraft encounters the auroral plasma cavity at 1323 UT, when the electron density drops by a half order of magnitude to less than 1.4 cm^{-3}. Interference from the intense *Z* mode radiation below the electron cyclotron frequency hampered the digitization of the whistler mode cutoff between 1323 and 1329 UT, although there was a sufficient gradient in the whistler mode amplitude throughout most of this interval to indicate that the density remained below 1.3 ± 0.5 cm^{-3}. Very intense AKR is evident above 100 kHz throughout most of this interval. The apparent lower frequency cutoff of the AKR at 57 kHz from 1329 to 1340 UT is due to the saturation of the fourth band of the receiver by these intense emissions.

In this example the average electron density just poleward of the cavity (1321–1322 UT) is 6.2 cm^{-3}. The minimum cavity density of 0.16 cm^{-3} occurs at 1331 UT and is nearly $1\frac{1}{2}$ orders of magnitude below the polar cap values just prior to the onset of the cavity. This cavity, like the one in Figure 1, is a one-sided cavity. The whistler mode cutoff fades out at 1334 UT just below 4 kHz at an *L* shell value of 5.1. The last measured density value in the cavity is 0.17 cm^{-3}. The f_{UHR} emissions which begin at 1347 UT have been used to construct the electron density profile equatorward of the cavity. At 1347 UT the electron density is 604 cm^{-3}, and the *L* shell value is 3.5. The highly elevated plasma densities after 1347 UT indicate that the spacecraft has crossed into the plasmasphere. Again, although a steep equatorward edge is not seen in the density profile, the increased densities after 1347 UT indicate that the auroral cavity is a U-shaped structure.

Day 323, 1981. The spectrogram for November 19, 1981, in Figure 3*b* has been chosen to illustrate the small "step down" in the electron density profile just poleward of the main cavity, a common feature in many nightside auroral zone crossings. Unlike the previous example, the polar cap density profile is relatively smooth in comparison to the irregular cavity profile, and the wave emissions are less intense. The *Kp* index for this pass is 3. Again the spacecraft is approaching the auroral zone from the nightside polar cap in the northern hemisphere. The spacecraft encounters a region of slightly diminished plasma densities at 1941 UT, followed by a steep gradient in the density profile at 1945 UT. Sharp spikelike features at 1941 and 1943 UT are impulsive intensifications in the wave activity which have no observable magnetic component. These electrostatic bursts periodically obscure the whistler mode cutoff throughout this auroral zone crossing. *Z* mode radiation is again evident both inside and outside the cavity interval, and intense AKR above 90 kHz saturates the fourth band of the plasma wave receiver from 1900 UT to 1930 UT.

In this example the average electron density from 1939 UT to 1940 UT is 4.2 cm^{-3}. At 1941 UT the electron density falls below 3 cm^{-3} and remains relatively constant until the main cavity is encountered at 1945 UT when the density drops to 0.4 cm^{-3}. The minimum cavity density of 0.17 cm^{-3} occurs at 1946 UT, more than an order of magnitude lower than the average polar cap density values. The auroral density profile becomes irregular after 1947 UT, and the simultaneous occurrence of electrostatic bursts and *Z* mode radiation in the same frequency range makes it difficult to trace the whistler mode cutoff continuously in this interval. However, there is no indication of an increase in the density profile prior to 1953 UT when the auroral hiss emissions and the upper frequency cutoff are obscured by intense, impulsive electrostatic bursts. The last measured density value in the cavity is 0.30 cm^{-3}. Faint f_{UHR} emissions again indicate that the electron density profile increases rapidly equatorward of the cavity. Measured densities exceeding 450 cm^{-3} after 2006 UT are certainly plasmaspheric.

Day 120, 1982. The spectrogram in Figure 4*a* was chosen to illustrate a low-altitude pass through the nightside auroral zone in the southern hemisphere. The spacecraft passes through the dayside auroral region in the northern hemisphere at 1420 UT, crosses the magnetic equator at 1437 UT, and passes through the dayside auroral region in the southern hemisphere at 1455 UT. From 1500 to 1516 UT the spacecraft passes through the southern polar cap region at very low altitudes and encounters the southern auroral cavity at 1516 UT. The poleward and equatorward expansions of the typical auroral hiss funnel have been compressed because of the convergence of the *L* shells at these low altitudes. As in Figure 3*a*, the wave emissions are very intense at all frequencies for this pass. Enhancement techniques [*Persoon et al.*, 1983] were used to trace the whistler mode cutoff inside the cavity and over the polar cap where intense *Z* mode radiation tends to obscure the cutoff. Intense auroral hiss emissions contribute to the saturation of the third band of the receiver, indicated by an intermittent artificial upper frequency cutoff at 57 kHz between 1510 and 1515 UT. Very intense AKR is again present in the cavity, saturating the fourth band of the receiver from 1512 to 1530 UT. The *Kp* index for this pass is 5−.

This cavity interval was selected to illustrate a density depletion with a clearly defined equatorward edge. The density gradient at the poleward edge is the steeper and sharper, however. From 1513 to 1514 UT the average polar cap density value is 6.0 cm^{-3}. At 1514 UT the spacecraft encounters a modest drop in the electron density profile to 3.7 cm^{-3}, followed by a steep negative gradient in the density profile at 1516 UT when the electron density falls to 0.51 cm^{-3}, more than an order of magnitude below the average polar cap value. A minimum cavity density of 0.11 cm^{-3} is encountered at 1518 UT at an invariant latitude of 74°. The electron density profile inside the cavity is highly variable with many small density enhancements up to 0.51 cm^{-3}. The equatorward side of the cavity is not a steep density gradient. A gradual recovery in the density profile to more than an order of magnitude above the minimum cavity density occurs between 1527 UT and 1528 UT.

Day 128, 1982. The spectrogram for May 8, 1982, shown in Figure 4*b*, was selected to illustrate a low-altitude pass over the nightside auroral zone in both hemispheres within 2 hours. The spacecraft crosses the nightside auroral zone in the northern hemisphere at approximately 0638 UT and then

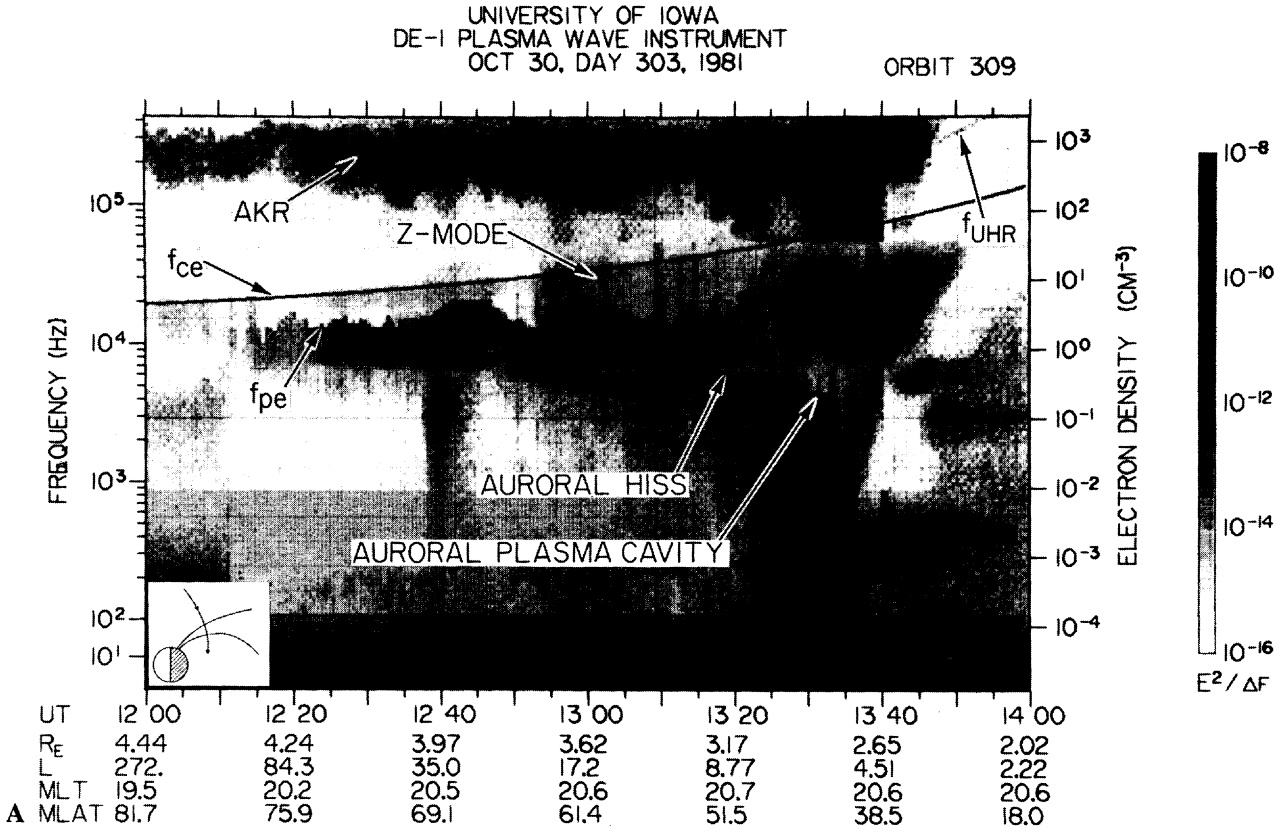

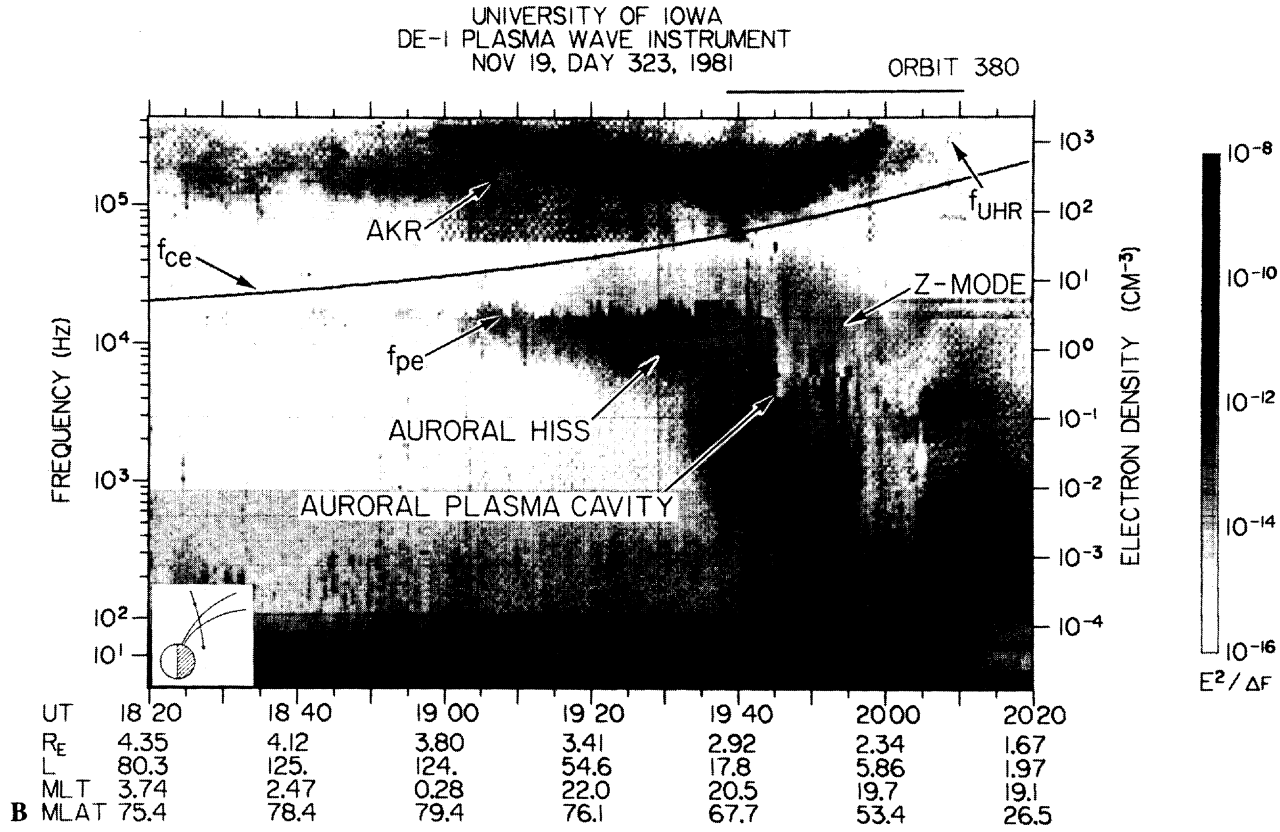

Fig. 3. Two representative electric field spectrograms illustrating passes through the nightside polar cap and auroral zone in the northern hemisphere. The spectrogram for October 30, 1981, in Figure 3*a* was chosen to illustrate a highly variable auroral density profile inside the cavity beginning at 1323 UT. The spectrogram for November 19, 1981, in Figure 3*b* illustrates a modest density depletion preceding the main cavity at 1945 UT. See the comment at the end of the Figure 1 caption pertaining to the f_{UHR} emissions in Figure 3.

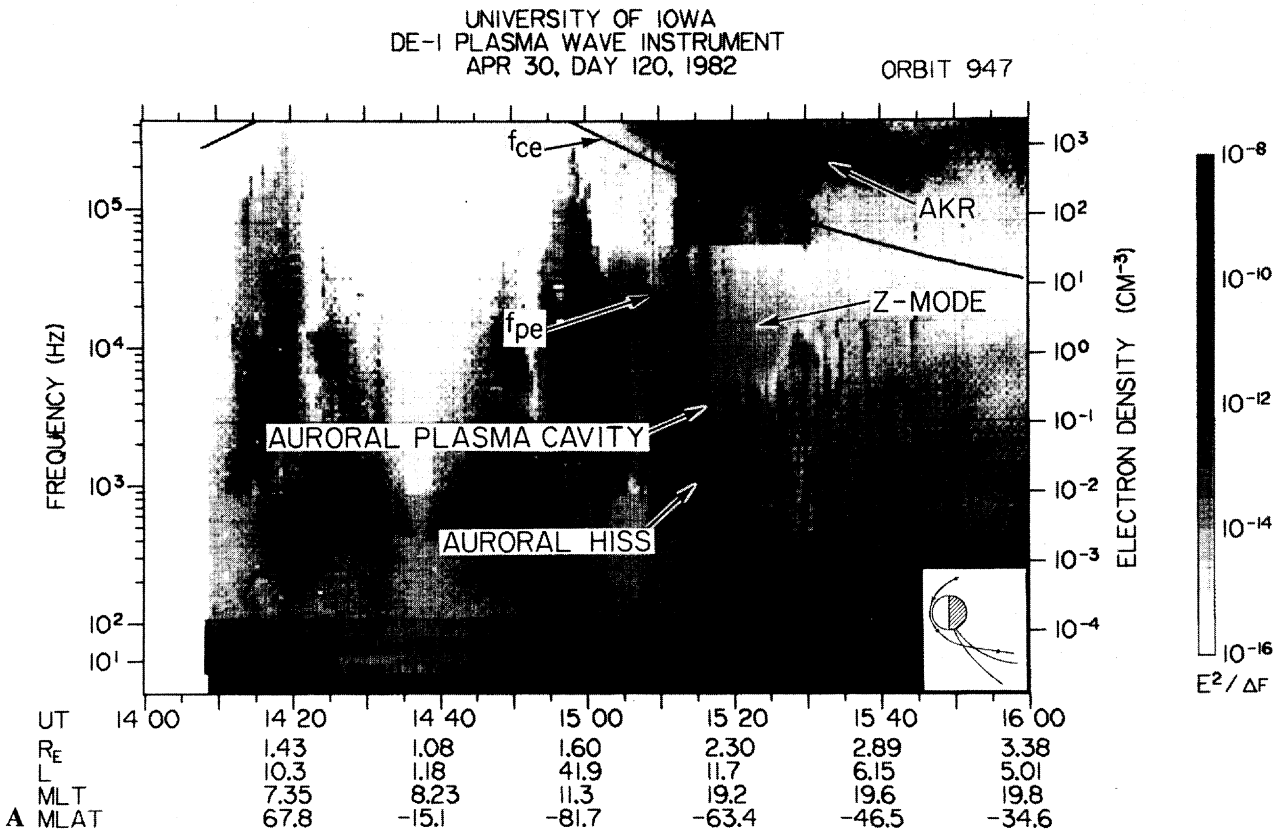

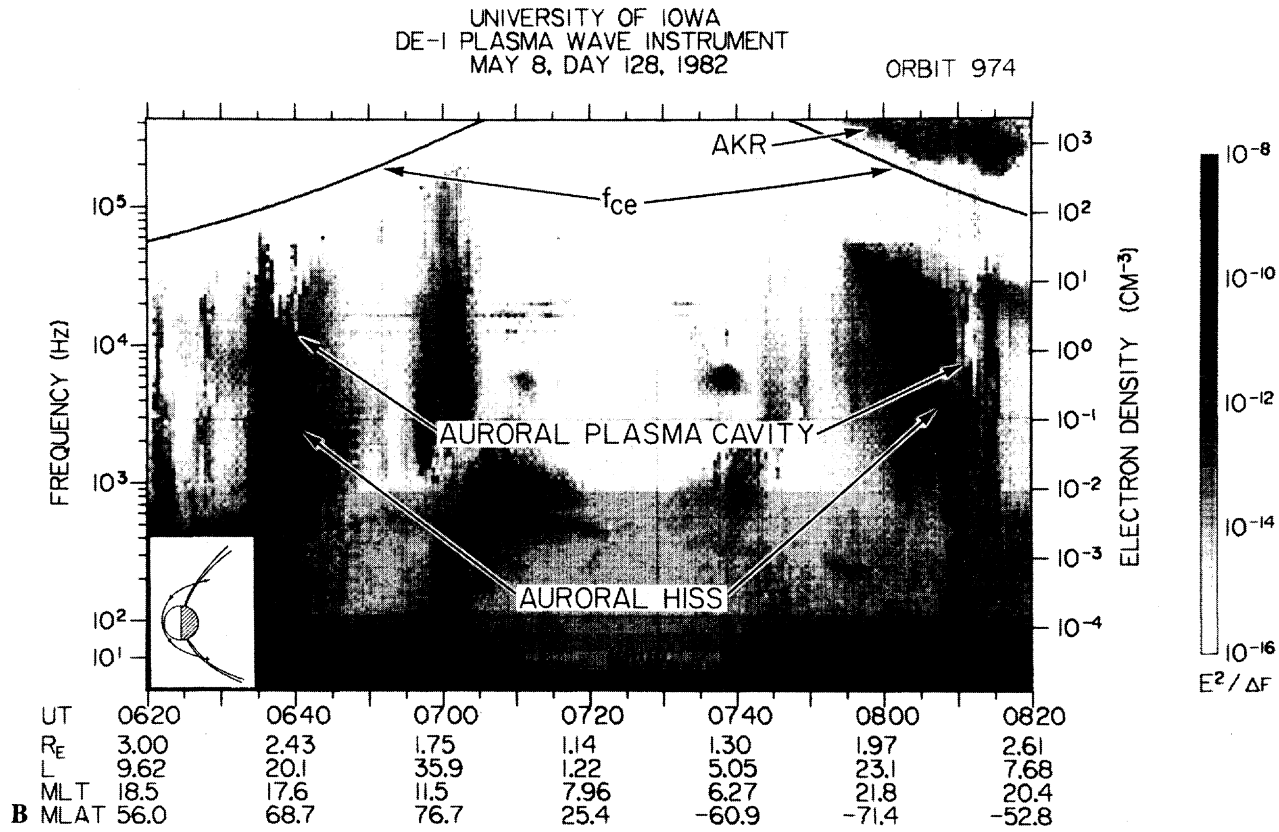

Fig. 4. Two representative spectrograms illustrating low-altitude passes through the nightside auroral zone in the southern hemisphere. The spectrogram for April 30, 1982 (Figure 4*a*), illustrates a southern auroral cavity with a well-defined poleward edge at 1516 UT and a modest positive gradient at the equatorward edge of the cavity after 1527 UT. The spectrogram for May 8, 1982 (Figure 4*b*), illustrates a low-altitude pass over the nightside auroral zone in both hemispheres with two-sided cavities occurring at 0641 UT and 0812 UT.

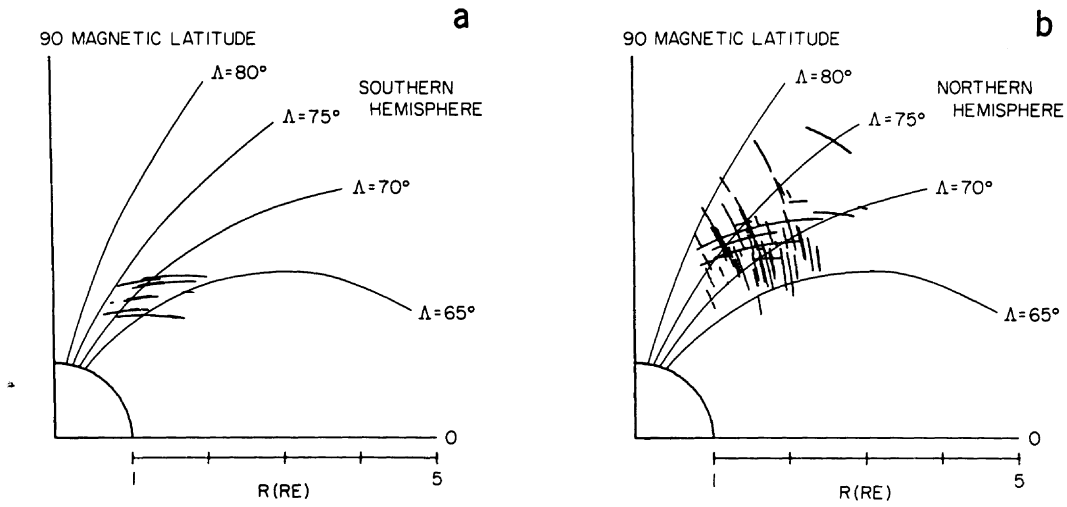

Fig. 5. The DE orbit traces are plotted for the 74 cavity intervals as a function of magnetic latitude and geocentric radial distance for the southern hemisphere (Figure 5*a*) and for the northern hemisphere (Figure 5*b*). Four representative field lines at invariant latitudes of 65°, 70°, 75°, and 80° are indicated on each plot. The average location of the auroral cavity is 70° ± 5° invariant latitude.

passes through the dayside auroral zone in the northern hemisphere at approximately 0700 UT, crossing the magnetic equator at 0725 UT. The spacecraft then passes through the southern dayside auroral zone and polar cap before arriving at the nightside auroral zone in the southern hemisphere at approximately 0808 UT. *Z* mode radiation and AKR are not observed in the northern auroral zone. However, intense AKR is present across the southern hemisphere, and *Z* mode radiation is evident both inside and outside the southern auroral cavity interval. The characteristic funnel shape of the auroral hiss emissions has again been compressed because of the convergence of the *L* shells at these low altitudes. The *Kp* index for this entire time interval is 1+.

The density gradient at the equatorward edge of the northern cavity is steep and clearly defined in this example. The electron density falls from 18.5 cm^{-3} at 0636 UT to 3.0 cm^{-3} at 0637 UT. A minimum cavity density of 1.8 cm^{-3} occurs at 0640 UT, and the spacecraft encounters the poleward edge of the cavity at 0641 UT, when the density suddenly rises to 21.0 cm^{-3}. The upper frequency cutoff of the hiss emissions fades out inside the northern polar cap, but the propagation of the cusp hiss emissions above 100 kHz at 0700 UT suggests that the density continues to rise as the spacecraft crosses the northern polar cap. The upper frequency cutoff of the hiss emissions in the southern polar cap region is sharp and smoothly varying. The average value of the polar cap electron densities between 0807 and 0808 UT is 6.0 cm^{-3}. Between 0809 and 1810 UT the spacecraft encounters a series of density depletions which reduce the electron density to 1.3 cm^{-3}, a half order of magnitude below the average density value just poleward of the cavity. A minimum density of 0.31 cm^{-3} is encountered at 0812 UT at an invariant latitude of 71°. The equatorward edge of this southern cavity is encountered at 0813 UT, when the density suddenly rises to 11.0 cm^{-3}.

3.2. *Frequency of Occurrence*

Because all of the PWI data for the first 3 months of the DE mission were available in spectrogram format, this subset of the data base was used to determine how frequently the auroral cavity is observed in the PWI data. From September 1981 through November 1981, Dynamics Explorer 1 crossed the nightside auroral field lines approximately 250 times. One hundred twenty-one auroral zone crossings, all in the northern hemisphere, were selected for which continuous data coverage from the long-wire electric antenna was available through the nightside auroral zone. Of these spectrograms, 72% showed evidence of substantial density depletions along auroral field lines. For the purposes of this study, a substantial density depletion is defined to be a sudden drop in the electron density of more than 40% below the electron density values just poleward of the low-density region. Eventually, there will be a sufficient PWI data base to determine how frequently the auroral cavity is observed in both hemispheres over all local times and seasons.

3.3. *The Location of the Auroral Cavity*

From the PWI data, 74 examples of auroral density depletions were selected for auroral zone passes where interference from other auroral wave emissions and Landau resonance effects were minimal. The upper frequency cutoff of the auroral hiss emissions for these examples was digitized with a minimum accuracy of ±3 frequency steps, corresponding to a maximum uncertainty in the electron density determination of ±40%. From the auroral density profile the poleward edge of the auroral cavity could be located in time with an accuracy of ±1 min for 93% of the cavity intervals. Densities at the poleward edge of the cavity were required to fall by more than 40%. For those auroral cavity examples for which a comparable equatorward recovery in the density profile could be determined, the equatorward edge of the auroral cavity was located in time with a minimum accuracy of ±90 s. The equatorward edge of the cavity could not be determined for 55% of the cavities.

Figures 5 and 6 are plots of the DE orbit traces for the 74 cavity intervals as a function of magnetic latitude and geocentric radial distance. Since the auroral oval and the

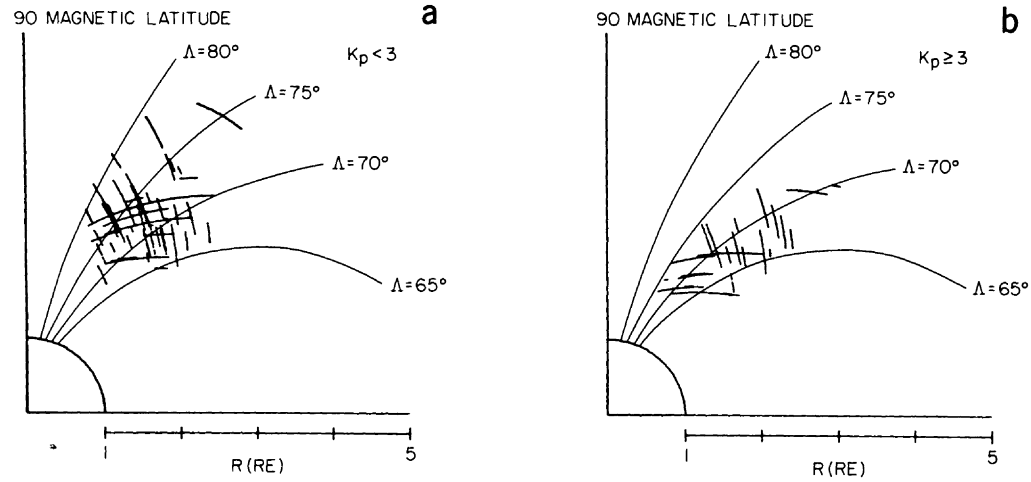

Fig. 6. Plots analogous to Figure 5 include the cavity intervals in both hemispheres for $Kp < 3$ (Figure 6*a*) and for $Kp \geq 3$ (Figure 6*b*). The equatorward shift of the auroral cavity with increasing geomagnetic activity is evident.

polar cap exhibit strong geomagnetic control and respond to changes in geomagnetic activity, similar influences are expected to affect the auroral cavity. To determine the extent of geomagnetic control over the location and width of the cavity, four representative auroral field lines at invariant latitudes of 65°, 70°, 75°, and 80° have been superimposed on the plots in Figures 5 and 6. The two plots in Figure 5 illustrate the location of the auroral cavity in the northern and southern hemispheres. Although auroral data in the southern hemisphere are restricted to the lower altitudes because of the spacecraft's orbit configuration in early 1982, it can be seen that the auroral cavity in both hemispheres most often occurs between 65° and 75° invariant latitude, in agreement with the ISIS 1 and Hawkeye observations of the auroral cavity in the AKR source region [*Benson and Calvert*, 1979; *Calvert*, 1981].

The auroral cavities which occur at invariant latitudes greater than 75° or less than 65° can be explained by examining the location of the auroral cavity with increasing geomagnetic activity. The plots in Figure 6 illustrate the location of the auroral cavity in both hemispheres for $Kp < 3$ and $Kp \geq 3$. For quiet conditions (Figure 6*a*), 71% of the auroral cavities have poleward edges at invariant latitudes greater than 72°. For more disturbed times (Figure 6*b*), 71% of the auroral cavities have poleward edges at invariant latitudes below 72°. No cavity data were available with a Kp index greater than 5−. The location of the poleward edge of the cavity has been used because the poleward edge can be determined with the greatest accuracy in nearly all of the cavity intervals. These results are consistent with the expansion of the polar cap and auroral oval in times of increasing geomagnetic activity.

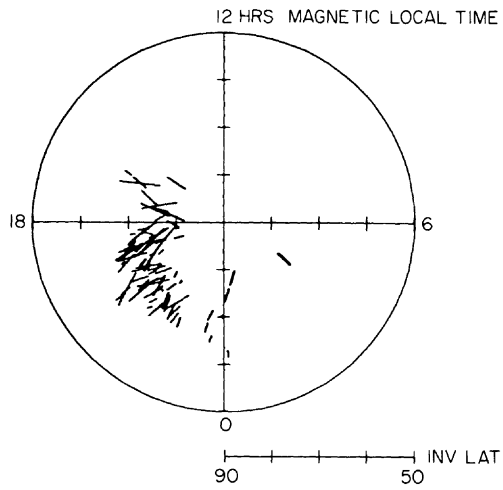

Fig. 7. Polar plot of the DE orbit trace for all 74 cavity intervals showing the location of the auroral cavity in invariant latitude and magnetic local time. The dearth of electron density depletions in the postmidnight auroral zone is due to the DE orbit configuration during the first 8 months of the mission. Data sampled in this study include all invariant latitudes above 50° in the late afternoon, evening, and early morning sectors.

Figure 7 is a polar plot of the DE orbit trace in invariant latitude and magnetic local time for the 74 cavity intervals. It was the purpose of this study to investigate regions of low electron density which occur on nightside auroral field lines. The majority of the auroral cavities presented in this study are found to cluster in the premidnight sector between 65° and 75° invariant latitude. The small number of cavities in the predawn sector is due to the configuration of the DE orbit during the time interval of this study. There are not sufficient data in this local time sector to determine the behavior of the auroral cavity in the predawn hours. The auroral cavities which occur in the predusk hours above 70° invariant latitude are low Kp events. No high Kp events in the afternoon sector were available to determine the latitudinal extent of the auroral cavity in the predusk hours.

3.4. *The Depth of the Auroral Cavity*

Because low plasma densities along auroral field lines play a significant role in the generation of the auroral kilometric radiation and the Z mode radiation commonly found in the auroral zone (see Figure 1), one objective of this study is to investigate the depth of the auroral cavity and to determine whether the densities in the cavity are sufficiently low to account for the presence of these plasma wave modes. Figures 8*a* and 8*b* are plots of the minimum density and the corresponding electron plasma frequency found in each cavity interval as a function of altitude for $Kp < 3$ and for $Kp \geq 3$. For U-shaped cavities the minimum density is likely to occur for more than one sweep of the step frequency receiver. In these cases, each minimum density value is

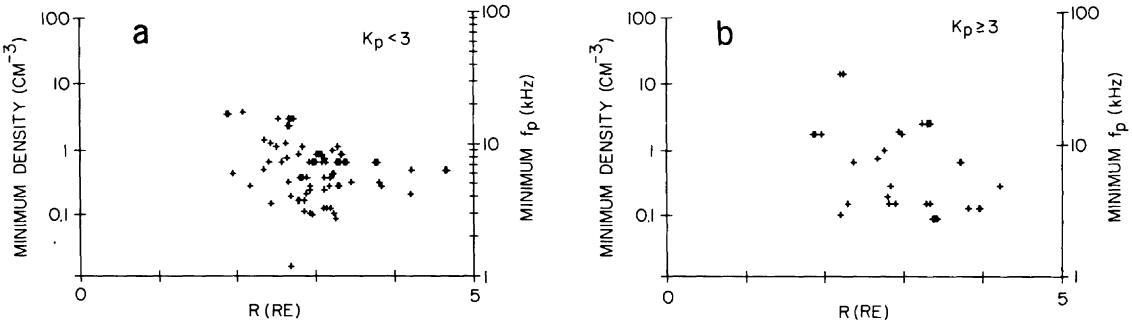

Fig. 8. Scatter plots of the minimum density and the corresponding electron plasma frequency of each cavity interval as a function of geocentric radial distance for $Kp < 3$ (Figure 8*a*) and for $Kp \geq 3$ (Figure 8*b*). When a minimum density value occurs more than once inside a cavity interval, each minimum density value is plotted independently as a function of geocentric radial distance. The minimum density in the auroral plasma cavity exhibits no strong altitude or Kp dependence.

independently plotted. Minimum cavity densities are found to vary from 0.02 cm^{-3} to 3.7 cm^{-3} for $Kp < 3$ and from 0.09 cm^{-3} to 14 cm^{-3} for $Kp \geq 3$ over the entire range of DE altitudes. There is no strong Kp or altitude dependence. Densities less than 1.0 cm^{-3} occur in 78% of the cavity intervals with a Kp index less than 3 and in 68% of the cavity intervals with a Kp index of 3 or more. The existence of very low densities, even at low altitudes, was anticipated on the basis of earlier ISIS 1 observations [see *Benson et al.*, 1980, Figure 5; *Benson*, 1981, Figure 12]. Auroral plasma densities are expected to be controlled by the auroral processes governing the ejection of ionospheric plasma.

Theoretical studies of the generation of AKR and Z mode radiation have stressed the importance of very low plasma densities in the auroral source regions [*Melrose*, 1976; *Wu and Lee*, 1979; *Grabbe et al.*, 1980; *James*, 1980; *Omidi and Gurnett*, 1982; *Melrose et al.*, 1984; *Omidi et al.*, 1984; *Omidi and Wu*, 1985, and references therein]. The ratio of the electron plasma frequency to the electron cyclotron frequency was found to be a significant factor in determining the growth rates of these two plasma wave modes. One objective of this study is to examine this critical frequency ratio in the auroral cavity to determine whether the low frequency ratios required in the source region by the cyclotron maser mechanism for the generation of these two wave modes are actually observed at DE altitudes. The minimum electron plasma frequencies found in the cavity intervals and the corresponding electron cyclotron frequencies were used to calculate the f_{pe}/f_{ce} ratios which are plotted in Figure 9 as a function of altitude for $Kp < 3$ and for $Kp \geq 3$. The range of f_{pe}/f_{ce} ratios is similar in both plots. The ratios vary from less than 0.02 to 0.4 at DE altitudes of 2–4.6 R_E geocentric. Ratios up to 1.3 were measured at 1.5 R_E by *Benson* [1985*a*] in the AKR source region. However, ratios below 0.2 often could not be resolved because of the low frequency limit of the ISIS 1 swept-frequency sounder [see *Benson*, 1985*a*, Figure 29]. The ratios determined from the PWI data are an extension of Benson's study to higher altitudes and lower frequency ratios. The lack of f_{pe}/f_{ce} ratios above 0.4 in Figure 9 is attributed to the restriction of data values to the minimum electron plasma frequency found in each cavity interval and to the limitations of the density analysis technique. Density measurements determined from an analysis of whistler mode wave propagation require that $f_{pe}/f_{ce} \ll 1$ (see section 2.1). The measured ratios are consistent with the values required by theory for the generation of AKR and Z mode radiation.

A survey of the PWI spectrograms for the 74 cavity intervals indicates a strong relationship between the occurrence of AKR and Z mode radiation and the occurrence of low-density regions in the nightside auroral zone. AKR was found to occur inside and poleward of the auroral cavity intervals in 97% of these intervals. The same PWI survey found that Z mode radiation occurred inside and immediately poleward of the auroral cavity in 78% of the cavity intervals. Only three of these Z mode events had f_{pe}/f_{ce} ratios of 0.2 or greater. The PWI observations of Z mode radiation, typically observed when $f_{pe}/f_{ce} < 0.2$ in the

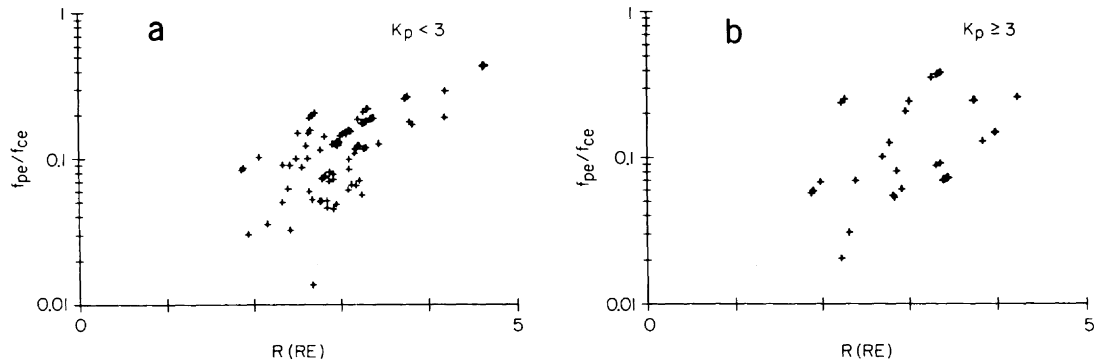

Fig. 9. Scatter plots of the ratio of the minimum electron plasma frequency to the corresponding electron cyclotron frequency plotted as a function of geocentric radial distance for $Kp < 3$ (Figure 9*a*) and for $Kp \geq 3$ (Figure 9*b*). Ratios are found to vary from 0.02 to 0.4 with no strong altitude or Kp dependence.

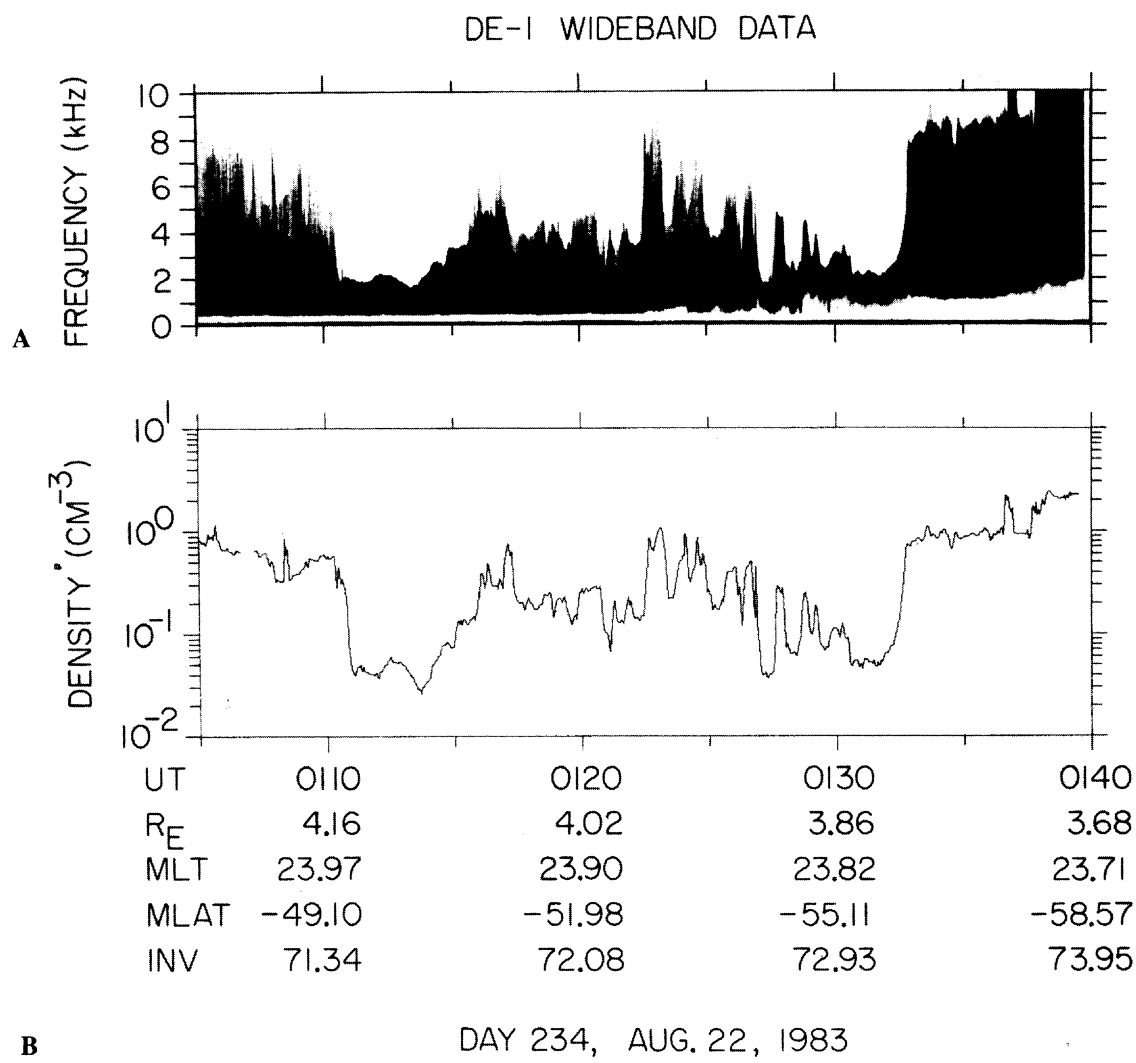

Fig. 10. An example of the DE wideband analog data, displayed in a condensed time frame, for an auroral zone crossing in the southern hemisphere on August 22, 1983 (Figure 10*a*). Also included is the high-resolution density profile derived from the digitized electron plasma frequency cutoff in the analog data (Figure 10*b*).

auroral cavity, are consistent with the cyclotron maser theory for the generation of Z mode radiation [*Omidi et al.*, 1984; *Omidi and Wu*, 1985]. Low f_{pe}/f_{ce} ratios have also been found in low-altitude ISIS 1 observations of weak and intense AKR [see *Benson*, 1985*a*, Figure 15] and in ISIS 1 observations of weak Z mode radiation at auroral latitudes, most commonly observed when $f_{pe}/f_{ce} \leq 0.3$ [see *Benson*, 1985*a*, Figures 9*g* and 16].

3.5. *Fine Structure in the Cavity*

The same analysis technique used to derive auroral density profiles from the step frequency correlator data (with a time resolution of 32 s) can also be used to derive high-resolution density profiles from the DE wideband data. The wideband analog data are processed through a spectrum analyzer and displayed on film in an expanded time mode (see Figure 12). The upper frequency cutoff of the hiss emissions is then digitized to the nearest 0.1 kHz for each half spin of the spacecraft (every 3 s). The resulting error in the density determination is less than 4%. Wideband coverage in the auroral zone was sporadic during the first year of the DE mission. The data base was further reduced by the requirement that the instrument be operating at a base frequency of 650 Hz with either the 10-kHz or the 40-kHz bandwidth in order to study the auroral hiss emissions. Only a few examples of low auroral density regions were digitized for the first 8 months of the mission. Later in the DE mission, greater wideband coverage was available for frequencies below 40 kHz. An example of the wideband data, displayed in a condensed time frame, is shown in Figure 10*a* for an auroral zone crossing at 4 R_E in the southern hemisphere on August 22, 1983. The frequency axis is linear, ranging from 0 kHz to 10 kHz. The baseband frequency at 650 Hz is clearly visible. The data span a 40-min time interval from 0100 to 0140 UT. The high-resolution density profile, derived from the digitized electron plasma frequency cutoff in the analog data, is presented in the log linear plot of Figure 10*b*.

The plasma wave data over the entire 410-kHz frequency range are shown in Figure 11. This PWI spectrogram includes the 40-min wideband interval shown in Figure 10*a*. The lowest latitudinal extent of this southern cavity occurs at 0111 UT at an invariant latitude of 71°. At 0133 UT the spacecraft crosses into the polar cap at an invariant latitude of 73°. This auroral plasma cavity occurs at the end of a

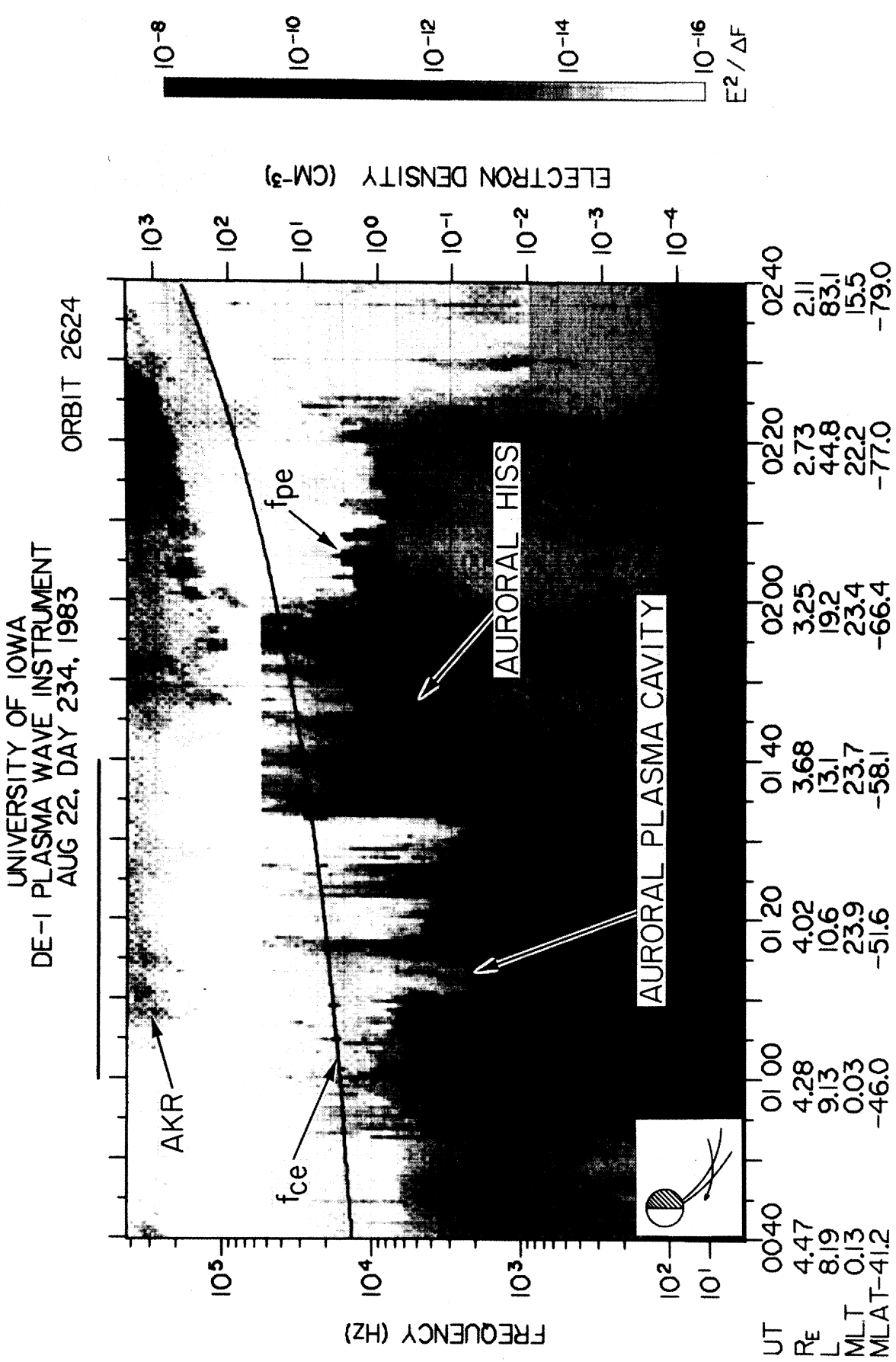

Fig. 11. An electric field spectrogram for the southern auroral zone crossing shown in Figure 10 illustrating the contraction of the auroral oval and the corresponding displacement of the cavity following a magnetic substorm.

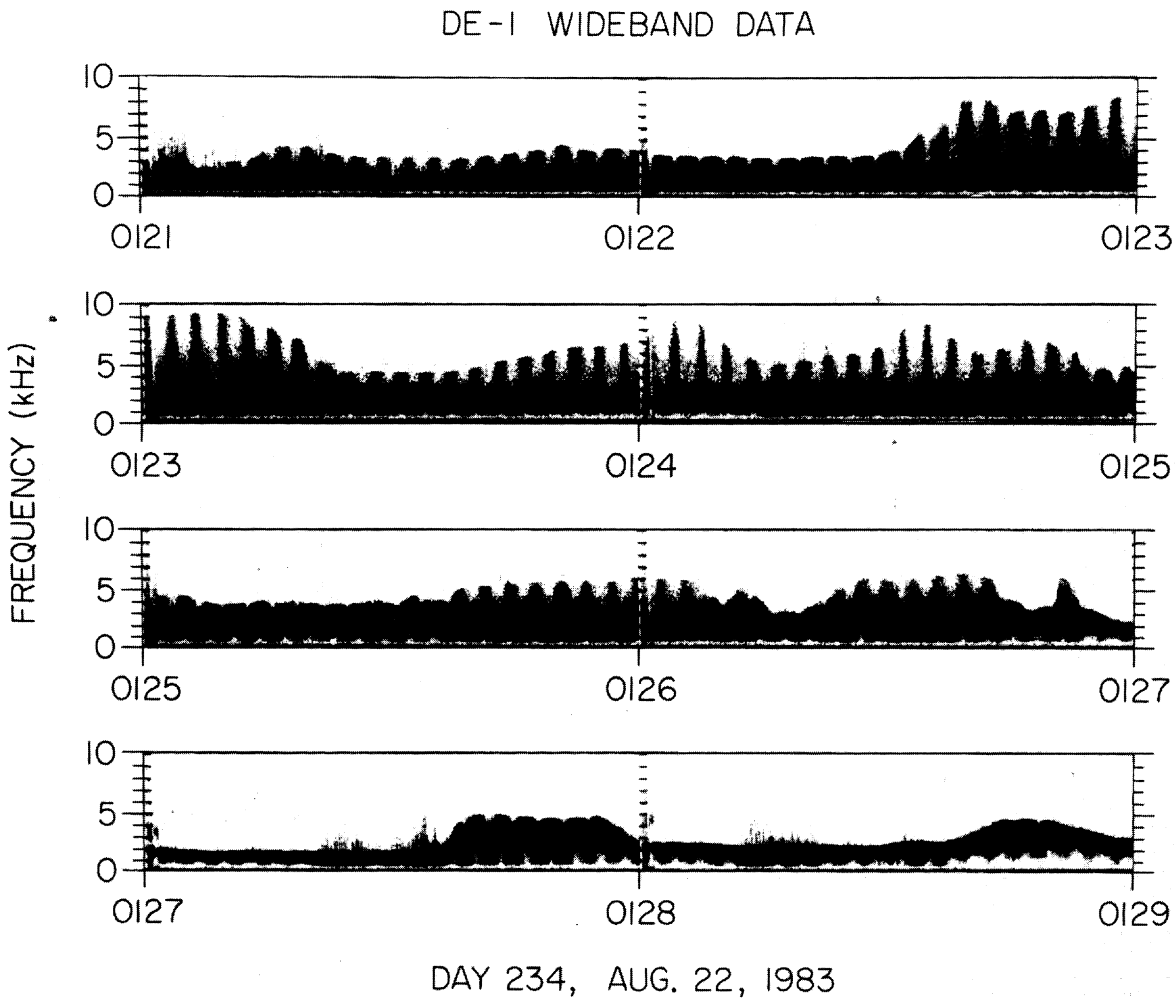

Fig. 12. Wideband analog data in an expanded time frame for the same southern auroral zone crossing shown in Figure 10 illustrating density structures inside the auroral cavity on very small spatial scales. The impulsive density enhancement at 0126:51 UT has a maximum width of 9 km.

magnetic substorm during which the *Kp* index climbed to 5− on the previous day. The *Kp* index fell from 4 to 2− just prior to this auroral zone crossing. The cavity itself appears to be divided into three parts, each separated by regions of density enhancements. A minimum density of 0.03 cm^{-3} occurs at 0114 UT. The artificial cutoff at 57 kHz both inside and poleward of the cavity in Figure 11 indicates a saturation of the third band of the frequency receiver by the intense hiss emissions.

In addition to verifying and improving the accuracy of the identification and scaling of the electron plasma frequency, the high-resolution wideband data enable us to examine fine structure inside the auroral cavity. Early low-altitude studies indicated that density profiles north of the equatorward edge of the main trough were highly variable [*Brace and Reddy*, 1965; *Muldrew*, 1965]. A survey of the PWI spectrograms reaffirmed the low-altitude observations with numerous examples of density fluctuations of a half order of magnitude or more occurring between successive sweeps of the step frequency receiver (refer to Figure 1).

The central part of the auroral plasma cavity in Figure 11 is characterized by rapid fluctuations in the density profile (see Figure 10*b*). These spatial/temporal density variations are very pronounced, with depletions and enhancements of an order of magnitude or more occurring on time scales of a half minute or less. These density structures are examined in greater detail in the DE wideband data, shown on an expanded time scale in Figure 12. The four panels in Figure 12 illustrate an expansion of the data in the 0121–0129 UT interval shown in Figure 10*a*. Several impulsive density enhancements, seen between 0123 UT and 0128 UT in Figure 10*b*, can be examined on a much smaller time scale in Figure 12. The hiss emissions in the wideband data show a strong modulation with each half-spin of the spacecraft (every 3 s). The upper frequency cutoff of the hiss emissions is clearly evident for each 3-s period throughout this interval. The average spacecraft velocity in this time interval is 3 km/s, nearly perpendicular to the auroral field lines. The large density enhancement which commences at 0122:35 UT and terminates at 0123:20 UT has a maximum width of 135 km. There is fine structure inside this auroral cavity on even smaller spatial scales. The density structure commencing at 0126:24 UT and the one commencing at 0127:38 UT are each 63 km across. The density structure at 0126:51 UT has a maximum width of 9 km. The 3-s time resolution of the wideband instrument puts an uncertainty of ±4.5 km on the

above measurements. These fine scale variations, as well as the large density variations on spatial scales of hundreds of kilometers, are probably field-aligned density structures, similar to the high-latitude field-aligned density irregularities observed at lower altitudes [*Muldrew*, 1969; *Muldrew and Vickrey*, 1982; *Benson*, 1985*b*]. Such sharp latitudinal density gradients have been associated with AKR harmonics and mode conversion [*Benson and Akasofu*, 1984; *Melrose et al.*, 1984; *Benson*, 1985*a*]. Numerous possibilities exist for producing these field-aligned density structures including shear-driven turbulence, instabilities associated with the steep density gradients in the cavity, and electric fields associated with the auroral acceleration process.

4. Plasma Energy and Ion Distributions in the Auroral Cavity

Since the auroral cavity is a common occurrence on nightside auroral field lines, the mechanism responsible for the depletion of plasma on these field lines will also be a common auroral phenomenon, subject to the same geomagnetic influences. The most likely mechanism for the transport of auroral plasma is the parallel electric field which accelerates the downgoing auroral electrons and the upgoing auroral ions. Upward directed ion beams have been commonly observed on auroral field lines [*Ghielmetti et al.*, 1978; *Gorney et al.*, 1981; *Yau et al.*, 1984]. *Chappell et al.* [1982] have shown that the ion outflows in the region of the auroral density cavity extend down to thermal energies. A typical auroral zone signature is a low-energy (<50 eV) conic or very broad angular distribution at the edges of a region of keV upward ion acceleration [*Klumpar et al.*, 1984; *Moore et al.*, 1985]. Statistical studies of EICS energetic ions [*Yau et al.*, 1984] have shown that upflowing H^+ and O^+ beams and conics with energies above 1 keV are commonly found at auroral latitudes and that these ion events exhibit the same latitudinal variations with changes in geomagnetic activity as the auroral density depletions. Upward directed parallel electric fields of 15 mV/m or less have been correlated with these upward directed ion beams and with auroral plasma density depletions just above 2 R_E [see *Temerin et al.*, 1981, Figure 14; *Mozer and Temerin*, 1983, Figure 6].

To determine how closely such upflowing auroral ions would correlate with the electron density depletions, a survey of the available RIMS and EICS summary data was conducted for the 74 cavity intervals. The RIMS summary data included plots of the estimated ion densities for five mass constituents and pitch angle–time spectrograms for H^+ and He^+. A positive correlation with the electron density depletions was assumed when an increase in the upflowing H^+ flux occurred within 1 min of the onset or poleward edge of the auroral cavity. A positive correlation was found between the low-energy upflowing H^+ ions and auroral density depletions for 85% of the intervals surveyed.

In the EICS summary plots, O^+ and H^+ ion fluxes are averaged over three energy ranges (<1 keV, 1–4 keV, 4–17 keV) in each of nine pitch angle bins. Flux is plotted for the pitch angle of the maximum flux in each of the three energy ranges. The summary plot survey made it possible to determine the correlation between auroral density depletions and the occurrence of energetic H^+ and O^+ beams and conics inside the cavity intervals. A positive correlation was assumed when upflowing ions with pitch angles exceeding 100° occurred within 1 min of the onset or poleward edge of the cavity. A positive correlation was found between low auroral densities and upflowing H^+ ions in the low-energy range (<1 keV) for 94% of the intervals surveyed. Eighty-six percent of the intervals showed a positive correlation between upflowing low-energy (<1 keV) O^+ ions and the poleward edge of the auroral cavity. Consistent with the results of *Yau et al.* [1984], it was found that the upflowing energetic (>1 keV) ions usually occurred equatorward of the low-energy (<1 keV) ions and are most often seen deep inside the auroral cavity. Less than 40% of these upflowing energetic ions were found near the poleward edge of the cavity. The low-energy (<1 keV) upflowing H^+ ions correlated well with the walls of the cavity, consistent with the RIMS results. These upflowing ions with a beamlike distribution appear to turn on at the poleward edge of the cavity and exist continuously throughout the cavity interval.

Since the summary plots are primarily designed to display only the most prominent features of the data, the existence of a positive correlation between upflowing ions and low auroral plasma densities for approximately 90% of the cavity intervals is an encouraging indication that the mechanisms responsible for the creation of auroral ion beams and the auroral plasma cavity are of a common origin. Several examples of H^+ and O^+ pitch angle distributions in different energy ranges have been selected to show the close correspondence between these upflowing ions and low auroral electron densities. Also included are color-coded energy-time spectrograms for the auroral ions and electrons to illustrate changes in the auroral plasma energy inside the low-density regions. Each color plate is a nine-panel multiple data set for an individual auroral cavity event.

The top four panels of each plate show the H^+ and O^+ pitch angle distributions observed by EICS for a particular cavity interval. The panels are spin-time spectrograms for the H^+ and O^+ ions integrated over two energy ranges (<1 keV and 1–17 keV). The 0° spin phase angle (ram direction) is at the bottom of each EICS spectrogram. Ions coming up the magnetic field lines from a source below the spacecraft appear near 90° in these spectrograms. The time resolution is 24 s in Plates 1 and 3 and is 96 s in Plate 2. The units for the EICS spectrogram color code are integral number flux in $cm^{-2}\ s^{-1}\ sr^{-1}$.

The fifth and sixth panels of each plate show the low-energy (<250 eV) H^+ and (<50 eV) O^+ ion distributions observed by RIMS. Each of the RIMS spectrograms shows the data ordered with respect to the spacecraft spin angle, with the spacecraft ram direction in the center of each spectrogram (labeled RAM). For the auroral cavity examples discussed in this section, all from the northern hemisphere, ions coming up magnetic field lines from below will appear in a symmetric distribution about the dashed line near the top of each spectrogram. The RIMS spectrograms are color-coded according to integral number flux in units of $cm^{-2}\ s^{-1}\ sr^{-1}$.

The seventh and eighth panels of each plate show the precipitating electron energy flux and the upgoing ion energy flux measured by HAPI for the selected cavity intervals. The HAPI spectrograms show the electron energy flux and the total ion energy flux as a function of energy (in keV) along the vertical axis and time along the horizontal axis. The HAPI spectrograms are color-coded according to energy flux in units of ergs $cm^{-2}\ s^{-1}\ sr^{-1}\ eV^{-1}$.

The bottom panel of each plate is a log linear plot of the

electron density profile derived from the digitized electron plasma frequency cutoff of the auroral hiss emissions for the selected cavity interval. Electron density in cm^{-3} is plotted as a function of time and the corresponding spacecraft parameters, which are listed along the bottom of each plate.

4.1. *October 25, Day 298, 1981*

Plate 1 shows the multiple data set for day 298, October 25, 1981, from 1610 to 1730 UT. The plasma wave data for this auroral zone crossing are shown in Figure 1. The bottom panel of Plate 1 is the electron density profile derived from the electron plasma frequency cutoff of the auroral hiss emissions for this interval. A high-latitude density depression, with average density values 36% below the polar cap densities on either side, is seen from 1648 UT to 1650 UT. A second small density depression, with a 39% drop in the electron density, occurs just before 1658 UT. This small density depression precedes the main cavity, which begins at 1700 UT with a drop in the electron density of more than a half order of magnitude below the average polar cap values preceding 1658 UT. The upper frequency cutoff of the hiss emissions fades out at 1707 UT, but the higher densities derived from the upper hybrid resonance at 1718 UT indicate that this auroral plasma cavity is a U-shaped density structure. Since the last density value inside the cavity occurs at 1707 UT, this time is taken to be the "open" equatorward edge of the cavity.

The (<1 keV) H^+ and O^+ ions in the EICS data (panels 2 and 4) show a broad angular distribution commencing just before 1658 UT. The H^+ distribution (<1 keV) in panel 2 collapses into a field-aligned beam at 1702 UT and persists until 1707 UT. The O^+ conic distribution (<1 keV) in panel 4 also becomes beamlike at 1702 UT. The energetic O^+ distribution (>1 keV) in panel 3, which shows evidence of a conic distribution at 1700 UT, also collapses to a field-aligned beam at 1702 UT and persists until 1707 UT. There is similar indication of a field-aligned energetic H^+ beam in the same interval (panel 1), consistent with the upflowing ion energy fluxes shown in panel 8. There is a well-defined pattern of ion conics and beams in the cavity interval. The EICS data also indicate the presence of a second component in the auroral ion population, an energetic quasi-isotropic population in H^+ (panel 1).

The integral number flux, particularly for the low-energy H^+ ions, correlates well with the onset of the electron density depletions. In panel 5, the H^+ ions (<250 eV) measured by RIMS show a substantial increase in the number flux and a very broad angular distribution from 1648 UT to 1650 UT, which is well correlated with the onset of a high-latitude density depression in panel 9. A similar H^+ conical distribution appears again after 1657 UT in a region of depressed auroral electron densities immediately preceding the main cavity. At 1702 UT the H^+ distribution becomes beamlike and persists throughout the cavity interval. The signature is consistent with the H^+ distribution seen in panel 2. The low-energy (<50 eV) O^+ ions, shown in panel 6, exhibit a weak beamlike distribution at 1703 UT. However, the most intense flux of field-aligned O^+ is seen at higher energies above 1 keV (panel 3). The feature in the RIMS data (panels 5 and 6) which runs at a constant integral number flux between 1610 UT and 1655 UT near the field-aligned direction is due to the instrument's detection of ultraviolet photons. The onset of a cold rammed distribution of O^+ in panel 6 at 1714 UT indicates the plasmapause region. Densities obtained from the upper hybrid resonance after 1718 UT in panel 9 are plasmapheric.

Inverted-V electron precipitation bands with peak energies up to 15 keV have been observed at low altitudes in the evening and midnight sectors of the auroral zone [*Frank and Ackerson*, 1972, Plate 1]. These bands extend over several degrees in invariant latitude at auroral latitudes consistent with the location of the auroral plasma cavity during magnetically quiet periods. At altitudes well below the auroral hiss source region, *Gurnett and Frank* [1972] observed downgoing auroral hiss emissions associated with these intense fluxes of energetic (100 eV to several keV) precipitating electrons. A similar pattern of auroral electron precipitation is shown in panel 7 in association with the upward directed auroral hiss and the auroral plasma cavity observed in the PWI data. The HAPI data indicate the development of an increasingly energetic electron population with energies up to 1 keV at 1657 UT and a split in the electron population into two energy components at 1700 UT. An increase in the energy of the precipitating electrons up to 10 keV occurs at the poleward edge of the cavity. An energetic component of the upflowing ions does not appear until 1702 UT, and these energetic ions are present until 1707 UT (panel 8). The most intense upward directed ion fluxes in the HAPI data (1702–1707 UT) correspond to the appearance of energetic (>1 keV) ion beams in the EICS data (panels 1 and 3).

Electron density values in two energy bins (18 eV to 1.3 keV and 1.3 keV to 13.2 keV), derived from the HAPI data, indicate that the bulk of the auroral electron population (>75%) in the cavity interval has energies below 1.3 keV. This analysis does not include the thermal component of the precipitating electron population due to the presence of photoelectrons in this low-energy range. The H^+ and O^+ ion densities have also been estimated for different energy ranges, averaged over the cavity interval. RIMS estimates of H^+ between 7 eV and 250 eV are consistent with the EICS estimates of H^+ and O^+ with energies exceeding 150 eV. H^+ is the dominant ion species in this cavity interval. The consistency of these two ion density estimates, averaged over the entire cavity interval, indicates that the bulk of the auroral ion population measured by the RIMS and EICS instruments inside the plasma cavity has an average energy of a few hundred electron volts. These three density estimates are, within statistical error, consistent with the averaged PWI densities in the cavity interval, indicating that the thermal ions and electrons, if present, are minor components of the total plasma population.

4.2. *October 30, Day 303, 1981*

Plate 2 shows the multiple data set for day 303, October 30, 1981, from 1230 to 1350 UT. The plasma wave data for this auroral zone crossing are shown in Figure 3*a*. The bottom panel of Plate 2 is the electron density profile derived from the electron plasma frequency cutoff of the auroral hiss emissions for this time interval. A steep density gradient occurs at 1323 UT when the density falls from 6.8 cm^{-3} to 1.4 cm^{-3}. This initial density drop is followed by a series of density drops interrupted by several impulsive density enhancements until a minimum cavity density of 0.16 cm^{-3} is recorded at 1331 UT. No equatorward edge of the cavity can be determined for this pass, although the equatorward edge can be located sometime between 1334 and 1346 UT when

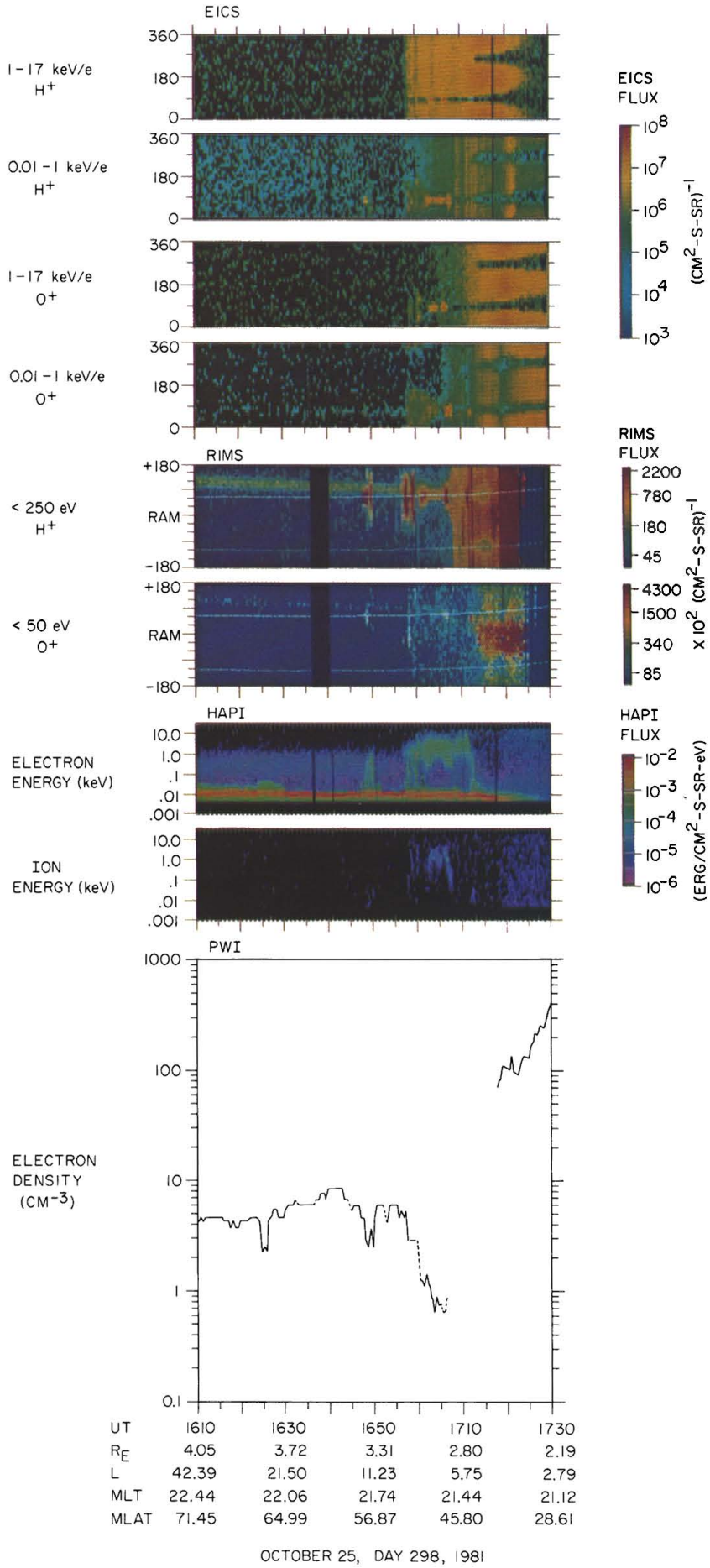

Plate 1. Nine-panel figure showing ion distributions and particle energies associated with an auroral electron depletion at 1700 UT on October 25, 1981. The panels illustrate the EICS energetic H^+ and O^+ distributions for two energy ranges (<1 keV and 1–17 keV), the RIMS low-energy H^+ and O^+ distributions, the HAPI precipitating electron and upgoing ion energy fluxes, and the electron density profile derived from the analysis of the plasma wave data.

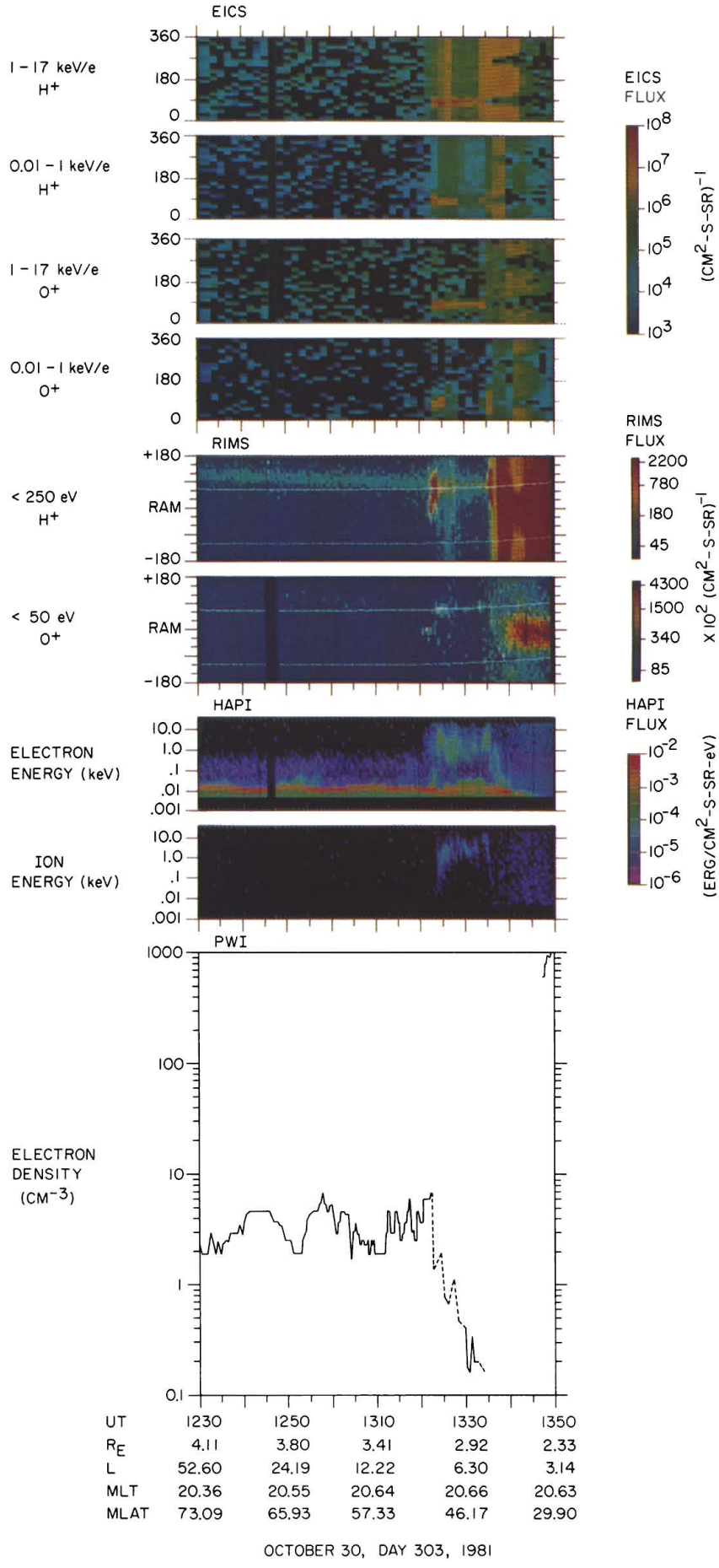

Plate 2. Nine-panel figure analogous to Plate 1 for an electron density depletion at 1323 UT on October 30, 1981.

higher plasmaspheric densities can be measured by digitizing the upper hybrid resonance (see Figure 3*a*). Since the plasma frequency cutoff in the auroral zone "fades out" at 1334 UT, this time is set as the "open" equatorward end of the cavity interval. This interval was selected to illustrate the temporal and spatial density variations in the plasma cavity.

The most significant ion signature in this cavity interval is seen in the energetic H^+ and O^+ distributions (panels 1 and 3). An abrupt onset of energetic field-aligned ions occurs in both ion species and in both energy ranges at 1323 UT. It is evident that although low-energy (<1 keV) ion beams are present in the cavity interval (panels 2 and 4), both species have a significant energetic component (1–17 keV), in agreement with the HAPI data in panel 8. These energetic H^+ and O^+ beams (panels 1 and 3) commence at 1323 UT and persist throughout the cavity interval.

A broad pitch angle distribution in the low-energy (<250 eV) H^+ ions is seen near the poleward edge of the main cavity just before 1323 UT (panel 5). By 1324 UT this conical distribution of H^+ ions has become field-aligned just inside the main auroral cavity. The field-aligned H^+ distribution becomes weak after 1329 UT, in agreement with the low-energy H^+ distribution shown in panel 2. A weak field-aligned flux of upflowing low-energy (<50 eV) O^+ is also evident near the poleward edge of the cavity in panel 6. The onset of a cold rammed distribution of O^+ at 1340 UT occurs at the plasmapause.

Energetic (10 keV) precipitating electrons are first observed immediately poleward of the auroral plasma cavity at 1321 UT (panel 7). However, the peak energies of this precipitating electron population, as well as the peak energies of the upflowing ion population (panel 8), occur just inside the cavity interval after 1323 UT. Both the energy and the energy flux of the upflowing ions and the precipitating electrons remain enhanced throughout the cavity interval. The most intense fluxes occur during the 1323–1329 UT interval when the digitization of the plasma frequency cutoff was the most difficult because of *Z* mode interference (see section 2.1).

The electron population in this cavity interval, derived from the HAPI data, again has an average energy below 1.3 keV, although there are two intervals (1324–1326 UT and 1335 UT) when the energetic electron population (>1.3 keV) is comparable to the low-energy component. The RIMS H^+ density estimates for energies below 250 eV and the EICS H^+ and O^+ density estimates for energies greater than 150 eV are consistent, indicating that the ion energy, averaged over the entire cavity interval, is of the order of a few hundred electron volts.

4.3. *November 19, Day 323, 1981*

Plate 3 shows the multiple data set for day 323, November 19, 1981, from 1855 to 2015 UT. The plasma wave data for this auroral zone crossing are shown in Figure 3*b*. The bottom panel of Plate 3 is the electron density profile for this cavity interval. A drop in the density profile of more than an order of magnitude below the average polar cap values occurs at 1945 UT, labeled as the onset or poleward edge of the auroral cavity. The equatorward edge of the cavity is not defined for this pass. Since the electron plasma frequency cutoff "fades out" at 1953 UT (see Figure 3*b*), this time determines the "open" equatorward end of the cavity interval. A minimum density of 0.17 cm^{-3} occurs at 1946 UT. Preceding this region of lowest auroral densities, there is a 4-min interval (1941–1945 UT) when the measured auroral densities of 2.3–3.0 cm^{-3} are only slightly less than the average polar cap density value of 4.2 cm^{-3} preceding 1940 UT. This cavity interval was selected because of this small depression in the density profile preceding the substantial negative gradient at the poleward edge of the main cavity.

Much of the ion activity in this interval occurs in the EICS data. Weak low-energy O^+ conic and beam distributions (panel 4) parallel the low-energy H^+ distributions in panel 2, but the O^+ integral flux is substantially lower, and the upflowing O^+ ion distribution does not persist throughout the cavity interval. A weak (<1 keV) H^+ conic distribution occurs poleward of the main cavity (1941–1945 UT), and a field-aligned (<1 keV) H^+ beam is evident throughout the cavity interval until 1956 UT (panel 2). Consistent with the results of *Yau et al.* [1984], the more energetic (>1 keV) H^+ and O^+ field-aligned beams occur equatorward of the low-energy ion events. Intense field-aligned distributions of energetic (>1 keV) H^+ and O^+ commence at 1947 UT and persist until 1953 UT (panels 1 and 3). However, although these energetic field-aligned ions are present inside the auroral cavity, they do not correlate with the onset of the cavity within the time resolution of both the EICS and PWI instruments for this pass.

Throughout the interval when energetic H^+ and O^+ beams are present (1947–1953 UT), only a very weak field-aligned H^+ distribution is seen at RIMS energies (<250 eV) in panel 5. No low-energy O^+ is evident in panel 6 for this time interval. The most striking feature in the RIMS data is the broad conical distribution of low-energy H^+ immediately poleward of the cavity between 1941 UT and 1945 UT, in a region of slightly depressed electron densities. This conical angular distribution of low-energy H^+ parallels the H^+ conics observed by EICS in panel 2. In addition, both the RIMS and the EICS data record a very weak, conical distribution of low-energy O^+ (panels 4 and 6) for the 1941–1945 UT interval, an interval when the recorded auroral electron densities are only slightly depressed. The plasmapause crossing is encountered at 2004 UT.

The HAPI data (panel 7) show the development of a very energetic (10 keV) precipitating electron population during the 1941–1945 UT interval. After 1945 UT this component of the electron population becomes slightly more energetic, with peak energies of nearly 20 keV occurring inside the cavity interval. These energetic precipitating electrons are present throughout the cavity interval. Prior to 1945 UT the ion energy flux in the upward direction is weak, and the ion energies fall below 100 eV (panel 8). At 1947 UT an energetic upflowing ion population with energies in excess of 1 keV appears.

Although the precipitating auroral electrons with energies greater than 1 keV become more energetic inside the auroral plasma cavity and although the percentage contribution of these energetic electrons to the total auroral electron population increases slightly inside the cavity interval, HAPI electron density estimates in the auroral cavity interval indicate that more than 85% of the auroral electron population is found at lower energies below 1.3 keV. Ion density estimates from the EICS data for ions with energies greater than 150 eV show individually varying but comparable contributions from H^+ and O^+ inside the main cavity. The estimates are consistent with the PWI auroral densities in the

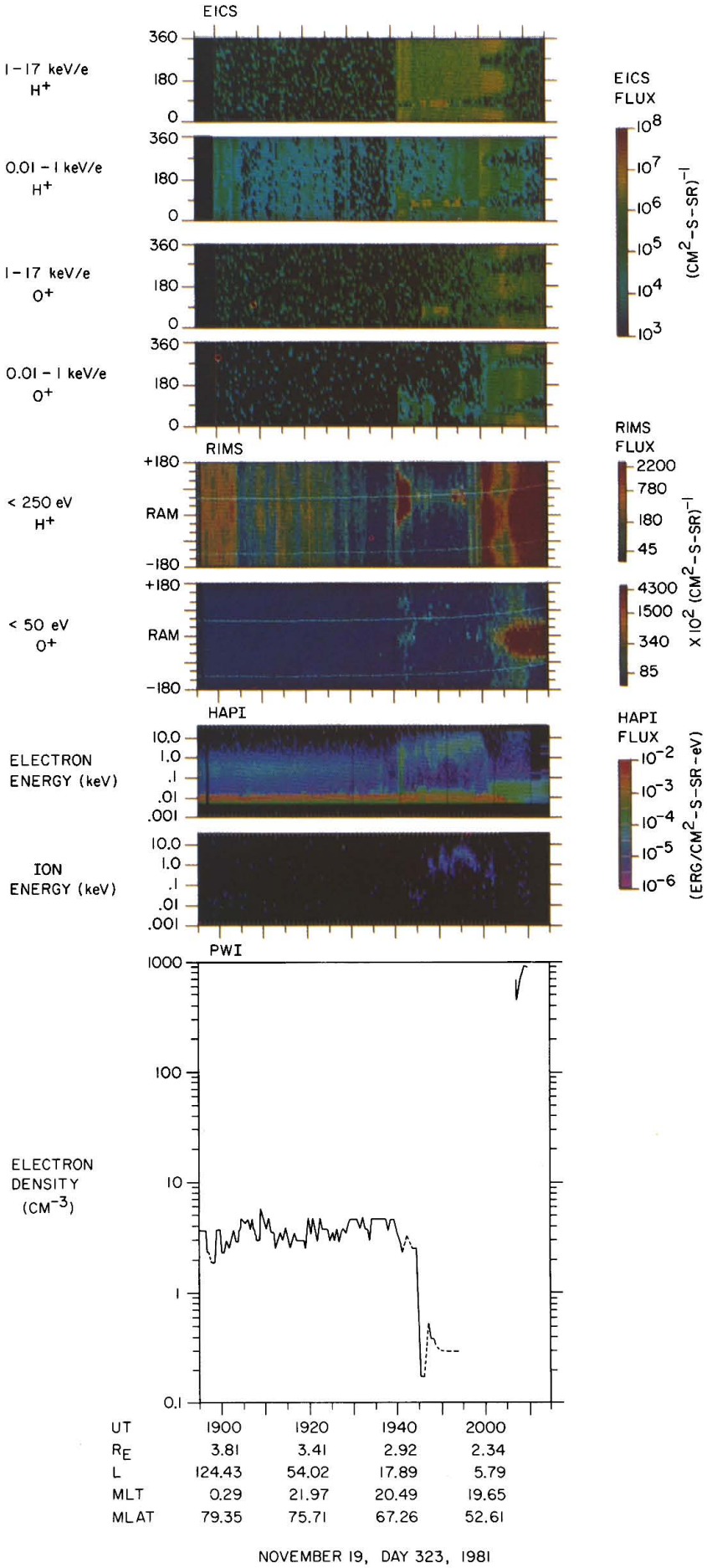

Plate 3. Nine-panel figure analogous to Plate 1 for an electron density depletion at 1945 UT on November 19, 1981.

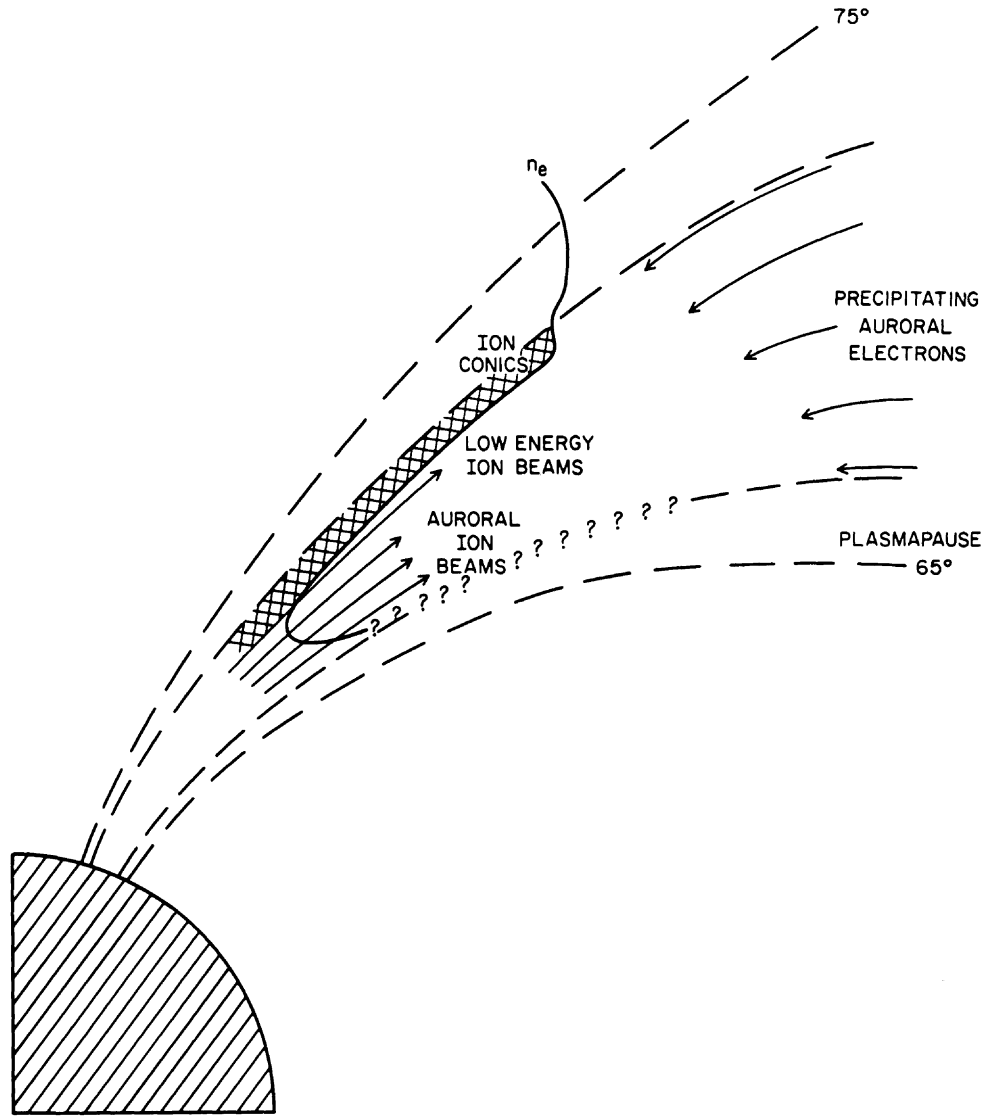

Fig. 13. The auroral plasma cavity, superimposed on dipole field lines, with the associated auroral particle distributions. Low-energy ion conic distributions are found at and above the poleward edge of the auroral cavity. Low-energy (<1 keV) ion beams, predominantly H^+, are highly correlated with the poleward edge, while ion beams with a wide range of energies are found inside the auroral cavity. Precipitating auroral electrons with energies in excess of 1 keV, found both inside and poleward of the auroral cavity, do not correlate with the onset of low auroral densities. However, the peak energies of the precipitating electron population do occur inside the auroral cavity interval.

same interval, indicating that auroral ions with energies below 150 eV constitute an insignificant component of the auroral ion population. This is in agreement with the RIMS density estimates for the H^+ ions with energies below 250 eV.

The results of the in-depth study of these three auroral cavity events are summarized in Figure 13. Broad conical distributions of low-energy H^+ are frequently found just poleward of the main cavity in a region of slightly diminished plasma densities. The collapse of these conical distributions into field-aligned ion beams with energies up to 1 keV correlates with the onset or poleward edge of the main cavity. Both low-energy (<1 keV) and energetic (>1 keV) upflowing auroral ions are found deep inside the main auroral cavity. The energetic ion beams do not usually correlate well with the poleward edge of the cavity. Density estimates of H^+ and O^+ in two energy ranges, averaged over the entire cavity interval, indicate that ions inside the auroral plasma cavity have energies of the order of one hundred to several hundred electron volts. A comparison between the EICS and RIMS ion density estimates and the PWI densities indicates that the thermal auroral ions, if present, are an insignificant component of the total population.

Although the energetic (>1 keV) precipitating auroral electrons do not correlate with the poleward edge of the auroral plasma cavity, the peak energies of the precipitating electron population do occur inside the cavity interval. There is an increase in the percentage of more energetic electrons to the total electron population inside the main cavity, but the bulk of the auroral electron population is found to have energies below 1.3 keV. The energetic electrons constitute, on the average, less than 25% of the total population. A comparison between the HAPI electron densities and the PWI densities indicates that the auroral electrons, like the ions, are predominantly nonthermal with energies in excess of 18 eV.

5. SUMMARY AND DISCUSSION

Discernible electron density depletions occur on nightside auroral field lines for more than 70% of the DE 1 auroral zone crossings during the first 3 months of the DE mission. Although the data base for the study of this common auroral density phenomenon is limited to 74 digitized auroral density profiles in the winter months, there is sufficient consistency in the results to draw some preliminary conclusions regarding auroral density depletions at DE altitudes.

The position of the auroral cavity in the PWI data in invariant latitude and local time correlates well with Hawkeye and S3-3 observations of the auroral plasma cavity [*Calvert*, 1981; *Temerin*, 1984] and with low-altitude observations of significant density depletions in the AKR source region [*Benson and Calvert*, 1979; *Benson and Akasofu*, 1984]. The auroral cavities in this study are found to occur at all DE altitudes (2–4.7 R_E geocentric) at 70° ± 5° invariant latitude over a wide range of magnetic local times from the predusk hours into the early morning sector. The location of the poleward edge of the auroral cavity has been found to occur at high invariant latitudes above 72° for low Kp values ($Kp < 3$) and to move to lower invariant latitudes at times of higher geomagnetic activity ($Kp \geq 3$). No cavity data were available for very disturbed times ($Kp \geq 5$).

Uncertainties in the determination of auroral electron densities can be large because of whistler mode propagation effects in the auroral zone (section 2). Subject to these uncertainties, minimum densities in the auroral plasma cavity are found to vary from 0.02 to 14.0 cm^{-3} over the entire range of DE altitudes. Estimated uncertainties in the density analysis run as high as ±40%. The depth of the cavity (minimum density within the cavity) shows no strong altitude or Kp dependence. The cavity depth is expected to be controlled by the same auroral processes governing the acceleration of ionospheric ions along auroral field lines.

The ratio of the electron plasma frequency to the electron cyclotron frequency is a sensitive parameter in the generation of AKR and Z mode radiation [*Wu and Lee*, 1979; *Omidi et al.*, 1984; *Omidi and Wu*, 1985] and in observations of these wave modes in the auroral zone [*Benson*, 1985*a*]. The frequency ratio, calculated for the minimum electron plasma frequency value in each cavity interval, is found to vary from 0.02 to 0.4 over all DE altitudes. A survey of the cavity data indicates that AKR occurs simultaneously with low auroral electron densities in 97% of the cavity intervals. Z mode radiation was found to occur in 78% of the cavity intervals. Only three observations of Z mode radiation are found to occur in cavity intervals with a minimum f_{pe}/f_{ce} ratio of 0.2 or greater. The results are in good agreement with ISIS 1 observations and with the cyclotron maser theory for the generation of these wave emissions.

In the three auroral events examined in detail, the peak energies of the precipitating electron population are found to occur in the region of the auroral cavity, although the appearance of energetic (>1 keV) precipitating auroral electrons does not correlate with the onset of the plasma cavity. The energetic precipitating electrons (>1 keV) are an insignificant component of the total precipitating electron population in the polar cap region just poleward of the auroral density depletions. Inside the cavity the percentage contribution of the energetic electrons to the total population increases slightly. However, on the average, more than 75% of the total auroral electron population is found at energies below 1.3 keV inside the auroral cavity.

A survey of the EICS and RIMS summary plots indicates that upflowing low-energy (<1 keV) H^+ ions occur within 1 min of the onset or poleward edge of the main cavity in more than 90% of the cavity intervals. The results of this preliminary survey are verified in the analysis of three cavity intervals. Field-aligned or conical low-energy (<1 keV) H^+ ions are found at the poleward edge of each cavity. These ion fluxes often become weaker inside the cavity, but they persist throughout the cavity interval. Low-energy O^+ ions are not consistently detected in the cavity intervals. Energetic (>1 keV) ion beams are found inside the auroral plasma cavity in the region of lowest auroral electron densities. But it is the less energetic (<1 keV) ion distributions which are highly correlated with the onset of the cavity. There appears to be a correlation between low-energy ion conic distributions and slightly higher auroral densities near the poleward edge of the cavity. Lowest auroral densities are highly correlated with the field-aligned ion distributions. The parallel electric field, which drives the auroral ion beams, appears to be the most efficient mechanism for the transport of ionospheric plasma and the creation of electron density depletions.

To determine whether these observed ion beams create the auroral density depletions seen at DE altitudes, it is necessary to estimate the "undisturbed" density profile along an auroral field line in the absence of dynamic auroral processes which contribute to auroral density variations. In the region immediately poleward of the auroral zone, the energy fluxes of the precipitating electrons are significantly diminished, and the upward directed ion beams are not consistently observed. An estimation of the density in a flux tube in this region would provide an estimate of an "undisturbed" high-latitude density profile. *Persoon et al.* [1983] determined the altitudinal variation of the electron density profile in the polar cap region over the range of DE altitudes [see *Persoon et al.*, 1983, Figure 10]. The power law distribution, $n_e \propto R^{-3.85}$, is used to integrate the electron density in a typical flux tube poleward of the auroral plasma cavity and to obtain an estimate of the total density in an "undisturbed" high-latitude flux tube. A rough estimate of 10^{10} cm^{-2} is obtained for the total electron density along a high-latitude flux tube from 2 R_E to 4.7 R_E.

Inside the auroral cavity, typical field-aligned ion fluxes of 10^7 cm^{-2} s^{-1} sr^{-1} are observed in the EICS data with a maximum solid viewing angle of approximately 30° for 1-keV ions. For an ion acceleration source region below 2 R_E [*Chiu et al.*, 1983; *Ghielmetti et al.*, 1978; *Gorney et al.*, 1981] a typical flux of keV ions could significantly deplete the plasma in an auroral flux tube up to 4.7 R_E in tens of minutes. This time scale is consistent with the observed response time of the auroral boundaries to variations in substorm activity and the interplanetary field [*Craven and Frank*, 1985; *Nakai et al.*, 1986] and with the presumed response time of the auroral plasma cavity to these same factors. The consistency of the time scales for these auroral phenomena suggests that ions, accelerating along auroral field lines from a source region below 2 R_E, could account for the observed loss of plasma from these field lines.

The auroral plasma cavity, unlike the main ionospheric trough [*Muldrew*, 1965], is a high-altitude density phenomenon. Observations from the ISIS 1 satellite found no consistent pattern of auroral electron density depletions below

2000 km [*Benson and Calvert*, 1979; *Benson and Akasofu*, 1984]. The auroral plasma cavity is highly correlated with field-aligned distributions of upflowing ions, occurring on auroral field lines adjacent to a region of low-energy ion conics. Upward directed low-energy H^+ conic distributions have been previously observed at DE altitudes in the auroral zone. Using magnetically coincident ground-based radar and DE measurements to correlate low-energy H^+ and He^+ distributions with low-altitude observations of particle precipitation and plasma densities, *Green et al.* [1986] found a strong correlation between upward directed low-energy ion conics and enhanced *F* region densities in the low-altitude auroral zone. These same conic distributions have been consistently observed at the poleward edge of the auroral plasma cavity in the PWI data. In the subauroral region, *Green et al.* [1986] measured bidirectional conic distributions of low-energy ions along magnetic field lines which are coincident with the ionospheric trough region. Examples of these bidirectional conics can be seen in Plate 1, panel 5, after 1712 UT and in Plate 3, panel 5, after 2000 UT. The bidirectional conic distribution, which occurs in a mid-latitude region where no electron densities were available in the PWI data, terminates at the equatorward edge of the auroral zone [*Green et al.*, 1986]. Different physical processes in the auroral and mid-latitude regions would indicate that in theory the auroral plasma cavity and the main ionospheric trough are distinct density phenomena. However, the current study does not indicate whether the two density depletions are physically distinct. The technique of using whistler mode wave propagation effects to determine the electron density fails in the critical region between the auroral cavity and the mid-latitude trough. Whistler mode wave propagation equatorward of the cavity (see Figure 2) and the low intensity of the upper hybrid resonance on many of the mid-latitude passes hamper density analysis in this mid-latitude region. The data fail to verify whether the auroral cavity and the mid-latitude trough are distinct low-density structures, separated by a mid-latitude region of enhanced plasma densities, or whether the two density depletions merge into one broad density depression between the polar cap and the plasmapause. Further density analysis in this critical region needs to be done.

Further study of the PWI data will make it possible to extend the study of electron density depletions to the dayside of the magnetosphere and across the polar cap and to study the energy flux and ion distributions associated with density depletions which occur in other regions of the high-latitude magnetosphere. Diurnal variations in the auroral oval are expected to apply to auroral density depletions near local noon, if such depletions are found to occur in the dayside oval. It is also possible that auroral processes in the dayside oval could result in enhanced auroral densities in this region. A preliminary survey of the early PWI data indicates that density depletions occurring inside the polar cap or at dayside auroral latitudes are not as deep, as broad, or as predictable as the auroral cavity. It is expected that the ion distributions inside these density depletions will be significantly different as well.

Acknowledgments. The plasma wave research at the University of Iowa was supported by the Dynamics Explorer program through NASA/GSFC grant NAG5-310 with additional support from NASA grants NGL-16-001-002, NGL-16-001-043, and through grant N00014-85-K-0404 with the Office of Naval Research. The work at Lockheed Palo Alto Laboratories was supported under NASA contract NAS5-28710. The work at Southwest Research Institute was supported under NASA contract NAS5-28711. The work at Marshall Space Flight Center was supported through the Dynamics Explorer program. Acknowledgments for the use of the RIMS data are expressed to C. R. Chappell, the RIMS PI.

The Editor thanks R. F. Benson and C. W. Carlson for their assistance in evaluating this paper.

REFERENCES

Andrews, M. K., and J. O. Thomas, Electron density distribution above the winter pole, *Nature*, *221*, 223, 1969.

Bates, H. F., A. E. Belon, and R. D. Hunsucker, Aurora and the poleward edge of the main ionospheric trough, *J. Geophys. Res.*, *78*, 648, 1973.

Benson, R. F., Auroral kilometric radiation source region observations from ISIS 1, in *Physics of Auroral Arc Formation*, *Geophys. Monogr. Ser.*, vol. 25, edited by S.-I. Akasofu and J. R. Kan, pp. 369–379, AGU, Washington, D.C., 1981.

Benson, R. F., Auroral kilometric radiation: Wave modes, harmonics, and source region electron density structures, *J. Geophys. Res.*, *90*, 2753, 1985*a*.

Benson, R. F., Field-aligned electron density irregularities near 500 km: Equator to polar cap topside sounder observations, *Radio Sci.*, *20*, 477, 1985*b*.

Benson, R. F., and S.-I. Akasofu, Auroral kilometric radiation/aurora correlation, *Radio Sci.*, *19*, 527, 1984.

Benson, R. F., and W. Calvert, ISIS 1 observations at the source of auroral kilometric radiation, *Geophys. Res. Lett.*, *6*, 479, 1979.

Benson, R. F., W. Calvert, and D. M. Klumpar, Simultaneous wave and particle observations in the auroral kilometric radiation source region, *Geophys. Res. Lett.*, *7*, 959, 1980.

Bowman, G. G., Ionization troughs below the *F*2-layer maximum, *Planet. Space Sci.*, *17*, 777, 1969.

Brace, L. H., and B. M. Reddy, Early electrostatic probe results from Explorer 22, *J. Geophys. Res.*, *70*, 5783, 1965.

Brace, L. H., and R. F. Theis, The behavior of the plasmapause at mid-latitudes: ISIS I Langmuir probe measurements, *J. Geophys. Res.*, *79*, 1871, 1974.

Brace, L. H., H. G. Mayr, and B. M. Reddy, The early effects of increasing solar activity upon the temperature and density in the 1000-km ionosphere, *J. Geophys. Res.*, *73*, 1607, 1968.

Burch, J. L., J. D. Winningham, V. A. Blevins, N. Eaker, W. C. Gibson, and R. A. Hoffman, High-altitude plasma instrument for Dynamics Explorer-A, *Space Sci. Instrum.*, *5*, 455, 1981.

Calvert, W., Steep horizontal gradients in the topside *F* layer, *J. Geophys. Res.*, *71*, 3665, 1966.

Calvert, W., The auroral plasma cavity, *Geophys. Res. Lett.*, *8*, 919, 1981.

Chappell, C. R., S. A. Fields, C. R. Baugher, J. H. Hoffman, W. B. Hanson, W. W. Wright, H. D. Hammack, G. R. Carignan, and A. F. Nagy, The retarding ion mass spectrometer on Dynamics Explorer-A, *Space Sci. Instrum.*, *5*, 477, 1981.

Chappell, C. R., J. L. Green, J. F. E. Johnson, and J. H. Waite, Jr., Pitch angle variations in magnetospheric thermal plasma—Initial observations from Dynamics Explorer-1, *Geophys. Res. Lett.*, *9*, 933, 1982.

Chiu, Y. T., J. M. Cornwall, J. F. Fennel, D. J. Gorney, and P. F. Mizera, Auroral plasmas in the evening sector: Satellite observations and theoretical interpretations, *Space Sci. Rev.*, *35*, 211, 1983.

Craven, J. D., and L. A. Frank, The temporal evolution of a small auroral substorm as viewed from high altitudes with Dynamics Explorer 1, *Geophys. Res. Lett.*, *12*, 465, 1985.

Frank, L. A., and K. L. Ackerson, Local-time survey of plasma at low altitudes over the auroral zones, *J. Geophys. Res.*, *77*, 4116, 1972.

Frank, L. A., et al., The theta aurora, *J. Geophys. Res.*, *91*, 3177, 1986.

Ghielmetti, A. G., R. G. Johnson, R. D. Sharp, and E. G. Shelley, The latitudinal, diurnal, and altitudinal distributions of upward flowing energetic ions of ionospheric origin, *Geophys. Res. Lett.*, *5*, 59, 1978.

Gorney, D. J., A. Clarke, D. Croley, J. Fennell, J. Luhmann, and P. Mizera, The distribution of ion beams and conics below 8000 km, *J. Geophys. Res.*, *86*, 83, 1981.

Grabbe, C. L., K. Papadopoulos, and P. J. Palmadesso, A coherent

nonlinear theory of auroral kilometric radiation, 1, Steady state model, *J. Geophys. Res.*, *85*, 3337, 1980.
Grebowsky, J. M., A. J. Chen, and H. A. Taylor, Jr., High-latitude troughs and the polar cap boundary, *J. Geophys. Res.*, *81*, 690, 1976.
Grebowsky, J. M., H. A. Taylor, Jr., and J. M. Lindsay, Location and source of ionospheric high latitude troughs, *Planet. Space Sci.*, *31*, 99, 1983.
Green, J. L., J. H. Waite, Jr., C. R. Chappell, M. O. Chandler, J. R. Doupnik, P. G. Richards, R. Heelis, S. D. Shawhan, and L. H. Brace, Observations of ionospheric magnetospheric coupling: DE and Chatanika coincidences, *J. Geophys. Res.*, *91*, 5803, 1986.
Gurnett, D. A., and L. A. Frank, VLF hiss and related plasma observations in the polar magnetosphere, *J. Geophys. Res.*, *77*, 172, 1972.
Gurnett, D. A., S. D. Shawhan, and R. R. Shaw, Auroral hiss, *Z* mode radiation, and auroral kilometric radiation in the polar magnetosphere: DE 1 observations, *J. Geophys. Res.*, *88*, 329, 1983.
Hagg, E. L., Electron densities of 8–100 electrons cm^{-3} deduced from Alouette II high-latitude ionograms, *Can. J. Phys.*, *45*, 27, 1967.
Helliwell, R. A., *Whistlers and Other Related Phenomena*, pp. 23–27, Stanford University Press, Stanford, Calif., 1965.
James, H. G., VLF saucers, *J. Geophys. Res.*, *81*, 501, 1976.
James, H. G., Direction-of-arrival measurements of auroral kilometric radiation and associated ELF data from ISIS 1, *J. Geophys. Res.*, *85*, 3367, 1980.
Klumpar, D. M., J. L. Burch, D. A. Gurnett, M. Sugiura, and J. H. Waite, Jr., The latitudinal structure of ion inverted V's, *Eos Trans. AGU*, *65*, 1060, 1984.
Liszka, L., The high-latitude trough in ionospheric electron content, *J. Atmos. Terr. Phys.*, *29*, 1243, 1967.
Melrose, D. B., An interpretation of Jupiter's decametric radiation and the terrestrial kilometric radiation as direct amplified gyroemission, *Astrophys. J.*, *207*, 651, 1976.
Melrose, D. B., R. G. Hewitt, and G. A. Dulk, Electron-cyclotron maser emission: Relative growth and damping rates for different modes and harmonics, *J. Geophys. Res.*, *89*, 897, 1984.
Miller, N. J., The main electron trough during the rising solar cycle, *J. Geophys. Res.*, *75*, 7175, 1970.
Miller, N. J., and L. H. Brace, Some winter characteristics of the northern high-latitude ionosphere, *J. Geophys. Res.*, *74*, 5752, 1969.
Moore, T. E., C. R. Chappell, M. Lockwood, and J. H. Waite, Jr., Superthermal ion signatures of auroral acceleration processes, *J. Geophys. Res.*, *90*, 1611, 1985.
Mosier, S. R., and D. A. Gurnett, VLF measurements of the Poynting flux along the geomagnetic field with the Injun 5 satellite, *J. Geophys. Res.*, *74*, 5675, 1969.
Mozer, F. S., and M. Temerin, Solitary waves and double layers as the source of parallel electric fields in the auroral acceleration region, in *High-Latitude Space Plasma Physics*, edited by B. Hultqvist and T. Hagfors, pp. 453–468, Plenum, New York, 1983.
Mozer, F. S., C. W. Carlson, M. K. Hudson, R. B. Torbet, B. Parady, J. Yatteau, and M. C. Kelley, Observations of paired electrostatic shocks in the polar magnetosphere, *Phys. Rev. Lett.*, *38*, 292, 1977.
Muldrew, D. B., *F* layer ionization troughs deduced from Alouette data, *J. Geophys. Res.*, *70*, 2635, 1965.
Muldrew, D. B., Nonvertical propagation and delayed-echo generation observed by the topside sounders, *Proc. IEEE*, *57*, 1097, 1969.
Muldrew, D. B., and J. F. Vickrey, High-latitude *F* region irregularities observed simultaneously with ISIS 1 and the Chatanika radar, *J. Geophys. Res.*, *87*, 8263, 1982.
Nakai, H., Y. Kamide, D. A. Hardy, and M. S. Gussenhoven, Time scales of expansion and contraction of the auroral oval, *J. Geophys. Res.*, *91*, 4427, 1986.
Nelms, G. L., Seasonal and diurnal variations of the distribution of electron density in the topside of the ionosphere, in *Electron Density Profiles in Ionosphere and Exosphere*, edited by J. Frihagen, pp. 358–386, North-Holland, Amsterdam, 1966.
Nelms, G. L., and G. E. K. Lockwood, Early results from the topside sounder in the Alouette II satellite, *Space Res.*, *7*, 604, 1967.
Nishida, A., Average structure and storm-time change of the polar topside ionosphere at sunspot minimum, *J. Geophys. Res.*, *72*, 6051, 1967.
Omidi, N., and D. A. Gurnett, Growth rate calculations of auroral kilometric radiation using the relativistic resonance condition, *J. Geophys. Res.*, *87*, 2377, 1982.
Omidi, N., and C. S. Wu, The effect of background plasma density on the growth of ordinary and *Z* mode emissions in the auroral zone, *J. Geophys. Res.*, *90*, 6641, 1985.
Omidi, N., C. S. Wu, and D. A. Gurnett, Generation of auroral kilometric and *Z* mode radiation by the cyclotron maser mechanism, *J. Geophys. Res.*, *89*, 883, 1984.
Persoon, A. M., D. A. Gurnett, and S. D. Shawhan, Polar cap electron densities from DE 1 plasma wave observations, *J. Geophys. Res.*, *88*, 10,123, 1983.
Reber, G., and G. R. Ellis, Cosmic radio-frequency radiation near one megacycle, *J. Geophys. Res.*, *61*, 1, 1956.
Rycroft, M. J., and J. O. Thomas, The magnetospheric plasmapause and the electron density trough at the Alouette I orbit, *Planet. Space Sci.*, *18*, 65, 1970.
Sharp, G. W., Midlatitude trough in the night ionosphere, *J. Geophys. Res.*, *71*, 1345, 1966.
Shawhan, S. D., D. A. Gurnett, D. L. Odem, R. A. Helliwell, and C. G. Park, The plasma wave and quasi-static electric field instrument (PWI) for Dynamics Explorer-A, *Space Sci. Instrum.*, *5*, 535, 1981.
Shelley, E. G., D. A. Simpson, T. C. Sanders, E. Hertzberg, H. Balsiger, and A. Ghielmetti, The energetic ion composition spectrometer (EICS) for the Dynamics Explorer-A, *Space Sci. Instrum.*, *5*, 443, 1981.
Smith, R. L., VLF observations of auroral beams as sources of a class of emissions, *Nature*, *224*, 351, 1969.
Stanley, G. M., Ground-based studies of the *F* region in the vicinity of the mid-latitude trough, *J. Geophys. Res.*, *71*, 5067, 1966.
Taylor, H. A., Jr., J. M. Grebowsky, and A. J. Chen, Ion composition irregularities and ionosphere-plasmasphere coupling: Observations of a high latitude ion trough, *J. Atmos. Terr. Phys.*, *37*, 613, 1975.
Temerin, M., Electron density and whistler mode propagation characteristics at 7000 km altitude in the auroral zone and polar cap, *J. Geophys. Res.*, *89*, 3945, 1984.
Temerin, M., C. Cattell, R. Lysak, M. Hudson, R. B. Torbert, F. S. Mozer, R. D. Sharp, and P. M. Kintner, The small-scale structure of electrostatic shocks, *J. Geophys. Res.*, *86*, 11,278, 1981.
Thomas, J. O., and M. K. Andrews, Transpolar exospheric plasma, *J. Geophys. Res.*, *73*, 7407, 1968.
Thomas, J. O., M. J. Rycroft, L. Colin, and K. L. Chan, The topside ionosphere, in *Electron Density Profiles in Ionosphere and Exosphere*, edited by J. Frihagen, pp. 322–357, North-Holland, Amsterdam, 1966.
Timleck, P., and G. L. Nelms, Electron densities less than 100 electron cm^{-3} in the topside ionosphere, *Proc. IEEE*, *57*, 1164, 1969.
Tulunay, Y., Magnetically symmetric detection of the mid-latitude electron density trough by Ariel 3 satellite, *J. Atmos. Terr. Phys.*, *34*, 1547, 1972.
Tulunay, Y., and J. Sayers, Characteristics of the mid-latitude trough as determined by the electron density experiment on Ariel III, *J. Atmos. Terr. Phys.*, *33*, 1737, 1971.
Wu, C. S., and L. C. Lee, A theory of the terrestrial kilometric radiation, *Astrophys. J.*, *230*, 621, 1979.
Yau, A. W., B. A. Whalen, W. K. Peterson, and E. G. Shelley, Distribution of upflowing ions in the high-altitude polar cap and auroral ionosphere, *J. Geophys. Res.*, *89*, 5507, 1984.

J. L. Burch, Department of Space Sciences, Southwest Research Institute, P. O. Drawer 28510, Division 15, San Antonio, TX 78284.
J. L. Green, National Space Science Data Center, NASA Goddard Space Flight Center, Greenbelt, MD 20771.
D. A. Gurnett and A. M. Persoon, Department of Physics and Astronomy, University of Iowa, Iowa City, IA 52242.
W. K. Peterson, Lockheed Missiles and Space Company, Inc., Palo Alto, CA 94304.
J. H. Waite, Jr., Space Science Laboratory, NASA Marshall Space Flight Center, Huntsville, AL 35812.

(Received December 17, 1986;
revised October 7, 1987;
accepted October 9, 1987.)